Characterization of the dynamic structures and interactions of Lewis X-carrying oligosaccharides and their clusters

Yan Gengwei

Doctor of Philosophy

Department of Functional Molecular Science
School of Physical Sciences
SOKENDAI (The Graduate University for Advanced Studies)

Characterization of the dynamic structures and interactions of Lewis X-carrying oligosaccharides and their clusters

Yan Gengwei

Department of Functional Molecular Science,

School of Physical Sciences,

SOKENDAI (The Graduate University for Advanced Studies)

Abstract

Oligosaccharides and their clusters are involved in a variety of biological processes exemplified by cellular communications and play crucial roles in multicellular organisms through carbohydrate-protein and carbohydrate-carbohydrate interactions. However, the physicochemical studies toward elucidation of the functional mechanisms of oligosaccharides have been precluded because their interactions are generally weak and transient and conventional recombinant techniques are not available for sample preparations.

It is widely supposed that the flexible property of oligosaccharides enables their conformational adaptability to various binding proteins, and in parallel, cause a loss of the conformational entropy upon the interaction coupled with their weak binding. Therefore, controlling the dynamic processes of oligosaccharides by designing their conformational spaces is a promising approach not only for improving binding affinities and specificities but also for better understanding of the detailed processes in biomolecular interactions involving oligosaccharides. The weak interactions of oligosaccharides also can be enhanced through formation of their clusters with multivalent binding ability as exemplified by multiple carbohydrate–carbohydrate interactions in their clustered states that mediate cell–cell interactions. To shed light on such dynamical interactions in the cell surface events as objectives in molecular science, it is necessary to employ appropriate models of the oligosaccharide clusters.

In this thesis, I addressed the dynamic interaction processes involving the Lewis X-derived oligosaccharides, including their conformational adaptation to the binding

partners as well as the multivalent recognition, by hybridizing biophysical, synthetic, and biochemical approaches. Lewis X is a trisaccharide, Galβ1-4(Fucα1-3)GlcNAcβ, displayed on various cell surfaces as a functional determinant. For example, Lewis X-carrying glycoproteins play a vital role in maintaining the stemness of neural stem cells. It has also been supposed that Lewis X clusters on cell surfaces can mediate cell–cell interactions through their homophilic binding.

In chapter 2, I chemically modified the dynamic conformations of the Lewis X oligosaccharide to improve its protein binding affinity for the cognate lectins. This has been successfully achieved based on exploration of the conformational space by employing NMR techniques combined with the molecular dynamics (MD) simulation. For adequately exploring the conformational space occupied by the Lewis X trisaccharide, I performed replica-exchange MD simulation in explicit water. To experimentally evaluate the simulation results, I obtained paramagnetism-assisted NMR data of this trisaccharide. Upon addition of Tm^{3+} ions to the chemically synthesized trisaccharide attached with a lanthanide-chelating tag, the NMR spectral change was observed due to pseudocontact shift (PCS), which can provide long-distance information in conformational characterization. The observed PCS data of the Lewis X trisaccharide were in excellent agreement with those back-calculated from the conformational ensemble derived from the replica-exchange MD simulation, thereby providing atomic descriptions of dynamic behaviors of this oligosaccharide in solution. The results in conjunction with the previously reported crystallographic data revealed the lectins selected rare conformers of Lewis X during binding processes.

This finding motivated me to re-design its conformational space for controlling its protein-binding properties. Indeed, chemical modification of the Lewis X trisaccharide to populate the bound conformations successfully improved the protein binding affinity. Thus, remodeling of the conformational spaces of oligosaccharides is an effective methodology for designing artificial oligosaccharides with improved efficacy through better understanding their conformational dynamics.

In chapter 3, I hybridized the Lewis X oligosaccharide with the self-assembled complex for creating neoglycoclusters, which possess structural homogeneity suitable for structural analyses and also potential functional ability through multivalent interaction. The glycosylated organic bidentate ligand was converted to glycoclusters displaying 24 Lewis X sugar moieties on its spherical scaffold through forming a metal-organic complex in the presence of Pd^{2+} ion. I demonstrated that the self-assembled glycocluster exhibited hyper-assembly through homophilic carbohydrate-carbohydrate interactions upon addition of Ca^{2+} ion. Furthermore, the well-defined Lewis X clusters enabled detailed NMR characterization of their interactions mediated by the oligosaccharides moieties. I successfully probed metal binding to the Lewis X-containing glycoclusters by observing paramagnetic relaxation enhancement. The NMR data revealed that the specific carbohydrate structure as well as their clustering form are prerequisite for the Ca^{2+}-mediated carbohydrate-carbohydrate interaction.

Moreover, in chapter 4, I created the novel glycoclusters composed of Lewis X-carrying neoglycolipids, in which the functional oligosaccharide units were

combined to acyl chains, as tools for controlling cellular functions. Using the synthetic Lewis X-carrying neoglycolipids, cell viability assays of neural stem cells before and after differentiation were performed. In this approach, it was demonstrated that the functional Lewis X glycotope connected to the fatty acid can evoke selective apoptosis of the neural stem cells before differentiation, while leaving the differentiated neuronal cells alive. The observed apoptosis was suppressed by the removal of lipid moiety or the fucose residue from the Lewis X-carrying neoglycolipid, indicating that the functional Lewis X group in a clustered form is a prerequisite for its apoptotic activity.

Thus, I employed synthetic approach integrated with biopysical techniques including NMR spectroscopy. Consequently, I could successfully design and create the neo-glycomolecules by hybridizing biomolecules and artificial molecules. The dynamical structures and assembly states of these neo-glycomolecules are artificially controlled in attempt to endow them with the higher affinity for target proteins, the Ca^{2+}-mediated hyper-assembling property, and the selective apoptotic activity. It is expected that these neo-glycomolecules can be useful tools for probing protein-carbohydrate interactions, carbohydrate-carbohydrate interactions, and cellular functional processes. It is also expected that the strategy I developed for creation and characterization of the neo-glycomolecules can be applicable for other biomolecules with structural flexibility and assembling properties.

Thesis contents:

Abstract

Thesis contents

Chapter 1. General introduction

1.1 Oligosaccharides in the biomolecular systems

1.2 Chemical and engineering studies of oligosaccharides

1.3 Physicochemical approach to oligosaccharides

1.4 Scope of this study

Chapter 2. Characterization of the dynamic conformation and interaction mode of Lewis X oligosaccharide

2.1 Introduction

2.2 Results and Discussion

2.3 Conclusions

2.4 Materials and Experiments

Chapter 3. NMR analysis of Ca^{2+}-mediated carbohydrate-carbohydrate interactions between Lewis X clusters

3.1 Introduction

3.2 Results and Discussion

3.3 Conclusions

3.4 Materials and Experiments

Chapter 4. Creation of Lewis X-carrying neoglycolipids for controlling cellular functions

4.1 Introduction

4.2 Results and Discussion

4.3 Conclusions

4.4 Materials and Experiments

Chapter 5. Conclusions and Perspective

Acknowledgments

Chapter 1. General introduction

1.1 Oligosaccharides in the biomolecular systems

Oligosaccharides and their clusters are involved in a variety of vital processes and play crucial roles in multicellular organisms. The functions of oligosaccharides are exerted commonly through carbohydrate-protein and carbohydrate-carbohydrate interactions (Figure 1). For example, oligosaccharides on cell membranes work as acceptors for various extracellular proteins [1-3], thereby mediating physiological and pathological events such as cellular communication and development, cancer metastasis, and viral infections. Growing evidence also indicates that oligosaccharide clusters on the cell surfaces provide supramolecular platforms for interactions among biomacromolecules including intrinsically disordered proteins involved in neurodegenerative diseases [4,5].

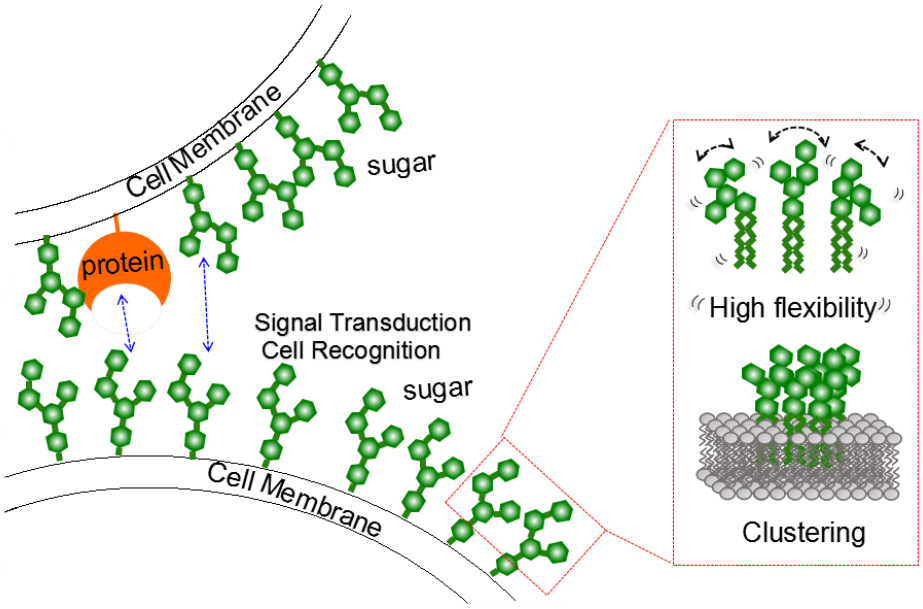

Figure 1. Oligosaccharides and their clusters on cell membranes.

Although a deeper understanding into the mechanisms underlying these oligosaccharide functions will promote biomolecular science into a new stage, the

physicochemical approach toward these challenges have been precluded because their interactions are generally weak and transient and conventional recombinant techniques are not available for sample preparations.

It is widely noted that carbohydrate chains are highly mobile in comparison with proteins. Glycosidic linkages, which are flexible C-O-C bonds between the carbohydrate residues, endow the oligosaccharides with numerous degrees of motional freedom. In addition to their conformational flexibility, the multi-antennary branched structures of oligosaccharides makes it difficult to explore their vast conformational spaces.

The flexible property of oligosaccharides enables their conformational adaptability to various binding proteins, and in parallel, cause a loss of the conformational entropy upon the interaction resulting in the weak binding [6,7]. Therefore, controlling the dynamic processes of oligosaccharides by designing their conformational spaces is a promising approach not only for biomolecular engineering aimed at improving binding affinities and specificities but also for the better understanding of the detailed processes in biomolecular interactions involving oligosaccharides.

The weak interactions of oligosaccharides can be enhanced through formation of their clusters with multivalent binding ability, by which the functional determinants cover a continuous surface promoting synergistic binding capability, as best exemplified by multiple carbohydrate–carbohydrate interactions in their clustered states that mediate cell–cell interactions [8,9]. To shed light on such dynamical

interactions in the cell surface events as objectives in molecular science, it is necessary to employ appropriate models of the oligosaccharide clusters.

1.2 Chemical and engineering studies of oligosaccharides

To characterize the dynamic structures and interactions of oligosaccharides and their clusters, I attempt to develop biophysical approaches combined with synthetic and biochemical approaches. In general, oligosaccharides derived from organisms are structurally heterogeneous and much less abundant than those needed for the biomolecular science studies. This is a significant bottleneck in biophysical investigation of oligosaccharides. Several attempts have been made to overexpress oligosaccharides with controlled glycoforms using cell engineering techniques [10,11]. However, such methods remain under development toward production of large quantities of oligosaccharides with tailored glycoforms [12]. Moreover, it is not possible to produce unnatural oligosaccharides by such biosynthetic methods.

By contrast, the synthetic approach is attractive because it enables to produce large quantities of oligosaccharides even with unnatural modifications [13,14]. Furthermore, a variety of oligosaccharide clusters, i.e. glycoclusters, can be synthesized by assembling carbohydrates onto artificial scaffolds such as nanoparticles, liposomes, polymers and dendrimers [15-18]. Bioactivities of synthetic glycoclusters and neoglycoconjugates were exemplified by inhibition of protein exotoxins and suppression of bacterial adhesion with functional oligosaccharides accumulated as dendrimers [19-21]. However, the physicochemical and structural

properties of such glycoclusters remain largely unknown, primarily because of the lack of an appropriate model system that combines structural homogeneity and the functional ability.

1.3 Physicochemical approach to oligosaccharides

One of the most useful methods of characterizing biomolecular structures and interactions is X-ray crystallography [22]. However, the conformational flexibility of oligosaccharides often precludes not only crystallization but also visualization of their structures. Nuclear magnetic resonance (NMR) spectroscopy is also a powerful technique to analyze structures and interactions of biomacromolecules in solution at atomic level [23]. Although NMR spectroscopy is potentially useful for the oligosaccharide studies, the NMR data, traditionally based on chemical shift, nuclear Overhauser effect (NOE) and spin-spin coupling (*J* coupling) [24-27], should be carefully interpreted because those are averaged over the dynamic conformational ensemble of oligosaccharides.

Recently, paramagnetism-assisted NMR approaches have been introduced in the fields of oligosaccharide structural studies [28-31]. Because of the large magnetic moment, unpaired electrons can affect the NMR signals originating from distal nuclei (as far as 40 Å) through through-space dipole interactions. Hence, observation of paramagnetic effects, such as pseudocontact shift (PCS) and paramagnetic relaxation enhancement (PRE), provides long-distance information of the molecular structures, which can be used to evaluate the overall conformations of oligosaccharides and their

dynamics in solution, complementing local conformation information derived from *J* couplings and NOE data. In our group, the paramagnetic NMR method has been applied to conformational analysis of flexible oligosaccharides by combining it with molecular dynamics (MD) simulation, thereby providing complementary views of to crystal structures regarding protein–oligosaccharide interactions [7,32,33].

1.4 Scope of this study

In this thesis, I attempted to characterize the dynamic conformations and interactions of Lewis X oligosaccharide, as a model of the biofunctional oligosaccharide, and to create artificial glycoclustrs displaying the Lewis X group useful for structural and functional analysis of the oligosaccharide assemblies. For this purpose, I employed a multilateral approach combining NMR spectroscopy with synthetic chemistry and computational simulation along with other biochemical and biophysical methods.

Lewis X is a branched trisaccharide, Galβ1-4(Fucα1-3)GlcNAcβ (Figure 2), displayed on various cell surfaces as a functional determinant [34-38]. For example, Lewis X-carrying glycoproteins play a vital role in maintaining the stemness of neural stem cells [37,38]. It has also been supposed that Lewis X clusters on cell surfaces can mediate cell–cell interactions through their homophilic bindings [36,39,40].

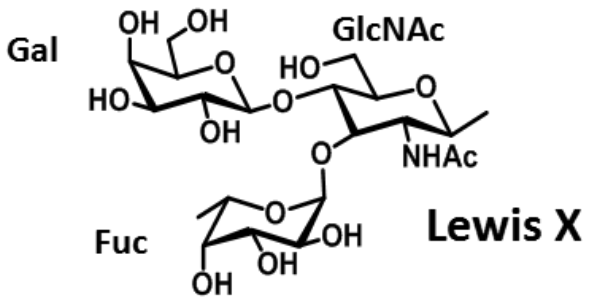

Figure 2. Representation of the Lewis X trisaccharide

To improve its protein binding affinity, I chemically modified the dynamic conformations of the Lewis X oligosaccharide. This has been successfully achieved based on exploration of the conformational space by employing paramagnetism-assisted NMR techniques combined with the all-atom MD simulation (Chapter 2). Moreover, Lewis X-carrying glycoclusters have been created by hybridizing self-assembled metal-organic complexes with the synthetic carbohydrate moieties for NMR characterization of carbohydrate-carbohydrate interactions (Chapter 3). For designing and creating glycoclusters having new functionality, Lewis X-carrying neoglycolipids were also synthesized as tools for controlling cellular functions (Chapter 4).

Thus, I successfully designed and created neo-glycomolecules containing the Lewis X group and thereby provides new tools useful for structural and biochemical studies of the oligosaccharides and their clusters.

References:

1. K. Drickamer and M.E. Taylor, Annu Rev Cell Biol. 1993, 9, 237–264.

2. N. Sharon and H. Lis, Springer. 2003.

3. H. J. Gabius, S. André, J. Jiménez-Barbero, A. Romero and D. Solis, Trends Biochem Sci. 2011, 36(6), 298–313.

4. K. Yanagisawa, Biochim. Biophys. Acta. 2007, 1768, 1943–1951.

5. T. Ariga, M.P. McDonald and R.K. Yu, J. Lipid Res. 2008, 49, 1157–1175.

6. M. Yagi-Utsumi and K. Kato, Glycoconjugate J. 2015, 32, 105-112 .

7. K. Kato, H. Yagi, T. Yamaguchi, Modern Magnetic Resonance, 2017, DOI: 10.1007/978-3-319-28275-6_35-1.

8. S. Hakomori, Pure and applied chemistry. 1991, 63, 473–482.

9. K. Iwabuchi, S. Yamamura, A. Prinetti, K. Handa and S. Hakomori, J. Biol. Chem. 1998, 273, 9130–9138.

10. Y. Kamiya, S. Yamamoto, Y. Chiba, Y. Jigami, K. Kato, J. Biomol. NMR 2011, 50, 397-401.

11. Y. Kamiya, K. Yanagi, T. Kitajima, T. Yamaguchi, Y. Chiba, K. Kato, Biomolecules 2013, 3, 108-123.

12. Y. Kamiya, T. Satoh, K. Kato, Curr Opin Struct Biol. 2014, 26, 44-53.

13. J. Shimabukuroa, H. Makyiod, T. Suzukia, Y. Nishikawa, M. Kawasaki, A. Imamura, H. Ishida, H. Ando, R. Kato, M. Kiso, Bioorg Med Chem. 2017, 25, 1132-1142

14. C. Chantarasrivong, A. Ueki, R. Ohyama, J. Unga, S. Nakamura, I. Nakanishi, Y. Higuchi, S. Kawakami, H. Ando, A. Imamura, H. Ishida, F. Yamashita, M. Kiso, M. Hashida, Mol. Pharmaceutics, 2017, 14, 1528–1537.

15. M. Delbianco, P. Bharate, S. Varela-Aramburu, and P. H. Seeberger, Chem. Rev. 2016, 116, 1693–1752.

16. T. Yamaguchi, T. Uno, Y. Uesaka, M. Yagi-Utsumi and K. Kato, Chem. Commun. 2013, 49, 1235–1237.

17. A. Bernardi, J. Jiménez-Barbero, A. Casnati, C. De Castr, T. Darbre, F. Fieschi, J. Finne, H. Funken, K.-E. Jaeger, M. Lahmann, T. K. Lindhorst, M. Marradi, P. Messner, A. Molinaro, P.l V. Murphy, C. Nativi, S. Oscarson, S. Penadés, F. Peri, R. J. Pieters, O. Renaudet, J.-L. Reymond, B. Richichi, J. Rojo, F. Sansone, C. Schäffer, W. B. Turnbull, T. Velasco-Torrijos, S. Vidal, S. Vincent, T. Wennekes, H. Zuilhof and A. Imberty, Chem. Soc. Rev. 2013, 42, 4709–4727.

18. M. Marradi, F. Chiodo, I. García and S. Penadés, Chem. Soc. Rev. 2013, 42, 4728–4745.

19. P. I. Kitov, J. M. Sadowska, G. Mulvey, G. D. Armstrong, H. Ling, N. S. Pannu, R. J. Read, D. R. Bundle, Nature. 2000, 10, 403, 669-672.

20. E. Fan, Z. Zhang, W. E. Minke, Z. Hou, C. L. M. J. Verlinde, W. G. J. Hol, J. Am. Chem. Soc. 2000, 122, 2663-2664.

21. S. Kötter, U. Krallmann-Wenzel, S. Ehlers, T. K. Lindhorst, J. Chem. Soc., Perkin Trans. 1, 1998, 2193-2200.

22. Y. Kamiya, T. Satoh and K. Kato , Curr. Opin. Struct. Biol. 2014, 26, 44–53.

23. J.F.G. Vliegenthart and R.J. Woods, Am. Chem. Soc. 2006.

24. J.F.G. Vliegenthart, Adv. Exp. Med. Biol. 1980, 125, 77–91.

25. T. Peters and B.M. Pinto, Curr. Opin. Struct. Biol. 1996, 6(5), 710–720.

26. J. Duus, C.H. Gotfredsen and K. Bock, Chem. Rev. 2000, 100(12), 4589–4614.

27. Y. Yamaguchi, T. Yamaguchi and K.Kato, Adv Neurobiol 2014, 9, 165–183.

28. Y. Zhang, T. Yamaguchi and K. Kato, Chem. Lett. 2013, 42(12), 1455–1462.

29. K. Kato and T. Yamaguchi, Glycoconj J 2015, 32, 505-513.

30. J. H. Prestegard and A. Eletsky, NMR in Glycoscience and Glycotechnology, 2017, pp. 123-149.

31. A. Canales and J. Jimenez-Barbero, NMR in Glycoscience and Glycotechnology, 2017, pp. 150-160.

32. T. Satoh, T. Yamaguchi, K. Kato, Molecules, 2015, 20, 2475-2491.

33. T. Suzuki, M. Kajino, S. Yanaka, T. Zhu, H. Yagi, T. Satoh, T. Yamaguchi, K. Kato, ChemBioChem 2017, 18, 396-410.

34. A. Capela and S. Temple, Neuron 2002, 35, 865–875.

35. E. Hennen and A. Faissner, Int. J. Biochem. Cell Biol. 2012, 44, 830–833.

36. N. Kojima, B. A. Fenderson, M. R. Stroud, R. I. Goldberg, R. Habermann, T. Toyokuni and S. Hakomori, Glycoconj. J. 1994, 11, 238–248.

37. H. Yagi, T. Saito, M. Yanagisawa, R. K. Yu and K. Kato, J. Biol. Chem. 2012, 287, 24356–24364.

38. H. Yagi and K. Kato, Glycoconjugate J. 2016, DOI:10.1007/s10719-016-9707-x.

39. S. Hanashima, K. Kato and Y. Yamaguchi, Chem. Commun. 2011, 47, 10800–10802.

40. A. Geyer, C. Gege and R. R. Schmidt, Angew. Chem. Int. Ed. 2000, 39, 3245–3249.

Chapter 2. Characterization of the dynamic conformation and interaction mode of Lewis X oligosaccharide

2.1 Introduction

Dynamic conformational properties of oligosaccharides in solution are significantly associated with the mechanisms of molecular recognition by carbohydrate recognition proteins collectively termed lectins, which involve conformational selection and induced-fit processes [1-4]. The interactions of oligosaccharides with their target proteins are accompanied by a significant loss of conformational entropy, explaining their generally low affinities to proteins. Therefore, control of the conformational spaces of oligosaccharides in free and protein-bound states is one of the effective approaches for improving their protein-binding properties.

Although the Lewis X trisaccharide, Galβ1-4(Fucα1-3)GlcNAc, was considered to exhibit a rigid "closed" conformation with limited structural fluctuation [5,6], its "open" conformations have recently been identified in its complexes with its cognate lectins by X-ray crystallographic analyses [7]. Here, I attempted to chemically manipulate the conformational space of the Lewis X trisaccharide on the basis of the knowledge of its dynamic conformations gained by NMR spectroscopy in conjunction with computational simulation. By this approach, I could successfully create a Lewis X analog with improved lectin-binding affinities.

2.2 Results and Discussion

For adequately exploring the conformational space occupied by the Lewis X trisaccharide, replica-exchange molecular dynamics (REMD) simulation was

performed with explicit water [8,9]. In this method, replicated simulations are run at different temperatures and the coordinates of replicas are exchanged during simulations to avoid being trapped into a local-energy-minimum state. For describing the dynamic conformations of the Lewis X, 64 replicas with a temperature distribution between 300 K and 500 K were used with a simulation time period of 53 ns for each replica (a total simulation time of 3.39 μs), obtaining torsion angle density maps of this trisaccharide (Figure 1).

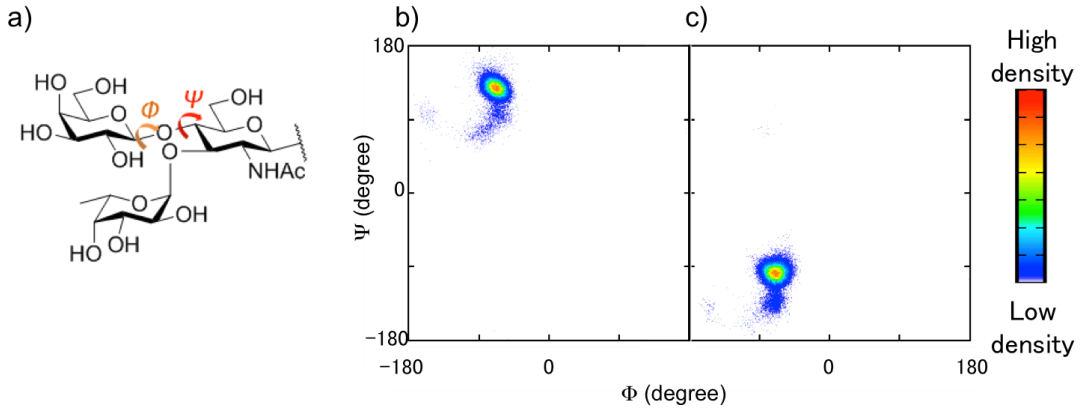

Figure 1. a) Structure of Lewis X trisaccharide and the simulated dihedral angles of b) the Galβ1-4GlcNAc and c) the Fucα1-3GlcNAc (Φ: O_5-C_1-O_1-C'_X, Ψ: C_1-O_1-C'_X-C'_{X-1}).

The torsion angles of the Gal-GlcNAc and Fuc-GlcNAc glycosidic linkages of this trisaccharide are mainly populated in clusters with averaged angles (Φ, ψ) = (-75°, 135°) and (-75°, -120°), respectively. This major conformation is close to a previously reported structure determined by the X-ray crystallographic analysis of the Lewis X trisaccharide [10], in which the stacking between the Fuc and Gal residues generates

the closed conformation. However, it should be noted that the simulated glycosidic torsion angle maps of the Lewis X trisaccharide exhibited broad energy minima more than just one single stable conformation. Furthermore, additional minor clusters are observed for the torsion angles of the Gal-GlcNAc linkage, (ϕ, ψ) = (-75°, 90°) and the Fuc-GlcNAc linkage, (ϕ, ψ) = (-65°, 130°). Major conformations in these clusters, are characterized by the exposure of the Gal and Fuc residues, i.e. open conformations.

For evaluating the result of the REMD simulation of the Lewis X trisaccharide, I employed the paramagnetism-assisted NMR method [11,12]. For PCS observation, I chemically synthesized the Lewis X trisaccharide tagged with a phenylenediamine-based lanthanide-chelating unit, as shown in Scheme 1. The reducing terminus of the oligosaccharide derivative was modified by selective azidation, and the phenylenediamine derivative was covalently attached by formation of a rigid amide linkage after reduction reaction of the synthesized trisaccharide.

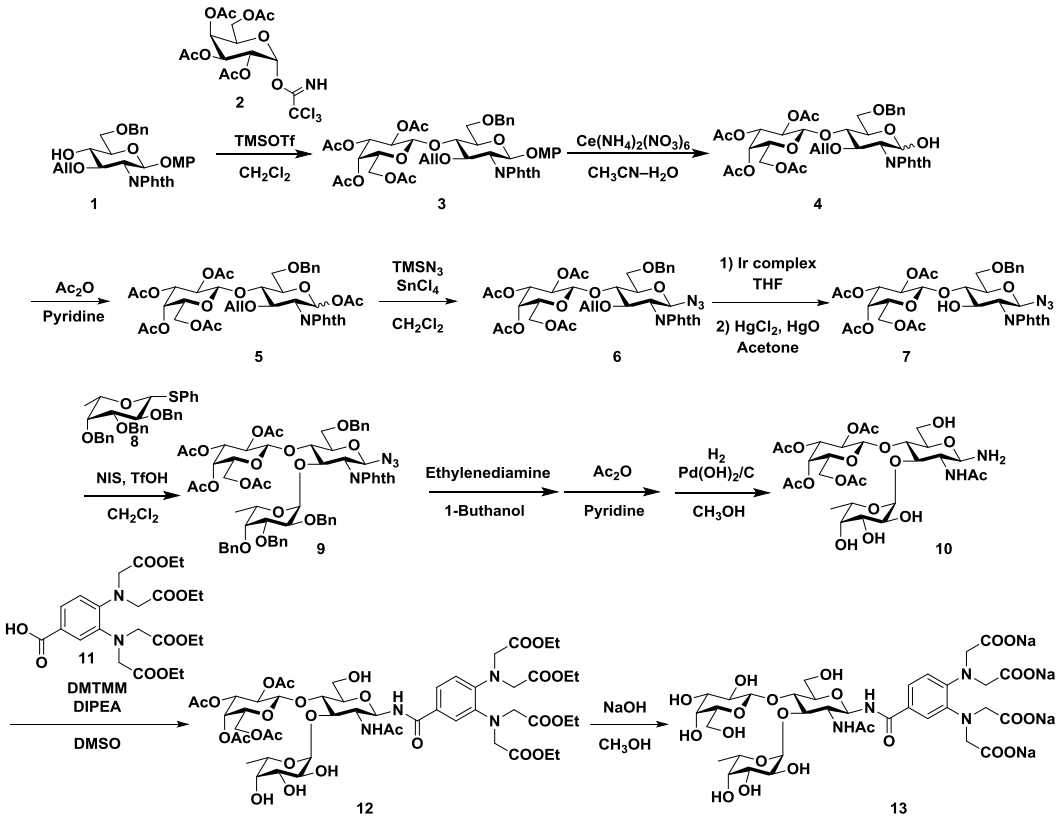

Scheme 1. Synthesis of the Lewis X trisaccharide tagged with the lanthanide-chelating unit.

To the D_2O solution of the tagged trisaccharide, paramagnetic Tm^{3+} ion was added so as to form a 1:1 complex. Stable complex formation was confirmed by observing disappearance of the original peaks and appearance of a new set of NMR peaks due to the lanthanide-induced PCSs (Figure 2) [13,14]. The PCS values of ^{1}H and ^{13}C were measured as the differences between the chemical shifts of the tagged trisaccharide complexed with Tm^{3+} ion and those observed with the diamagnetic La^{3+} ion in their ^{1}H-^{13}C HSQC spectra, as shown in Fugure 3a. Sequential assignments of the observed signals in ^{1}H-^{13}C HSQC spectrum of the trisaccharide were performed by employing DQF-COSY, HMBC and HSQC-TOCSY experiments. The

experimentally obtained PCS values were in good agreement with the values back calculated from the REMD data with a low Q value = 0.10 (Figure 3). Thus, the REMD-derived conformational ensemble of the Lewis X trisaccharide was experimentally validated.

$$\mathrm{PCS} = \frac{1}{12\pi \cdot r^3}\left[\Delta\chi_{\mathrm{ax}}(3\cos^2\theta - 1) + \frac{3}{2}\Delta\chi_{\mathrm{rh}}\sin^2\theta\cos 2\varphi\right]$$

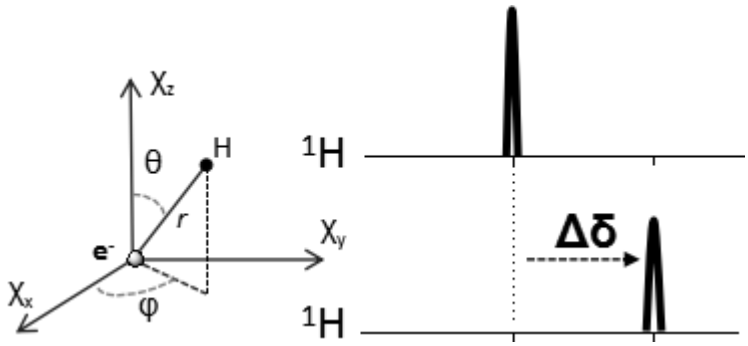

Figure 2. Observation of pseudocontact shift in NMR for the conformational analysis.

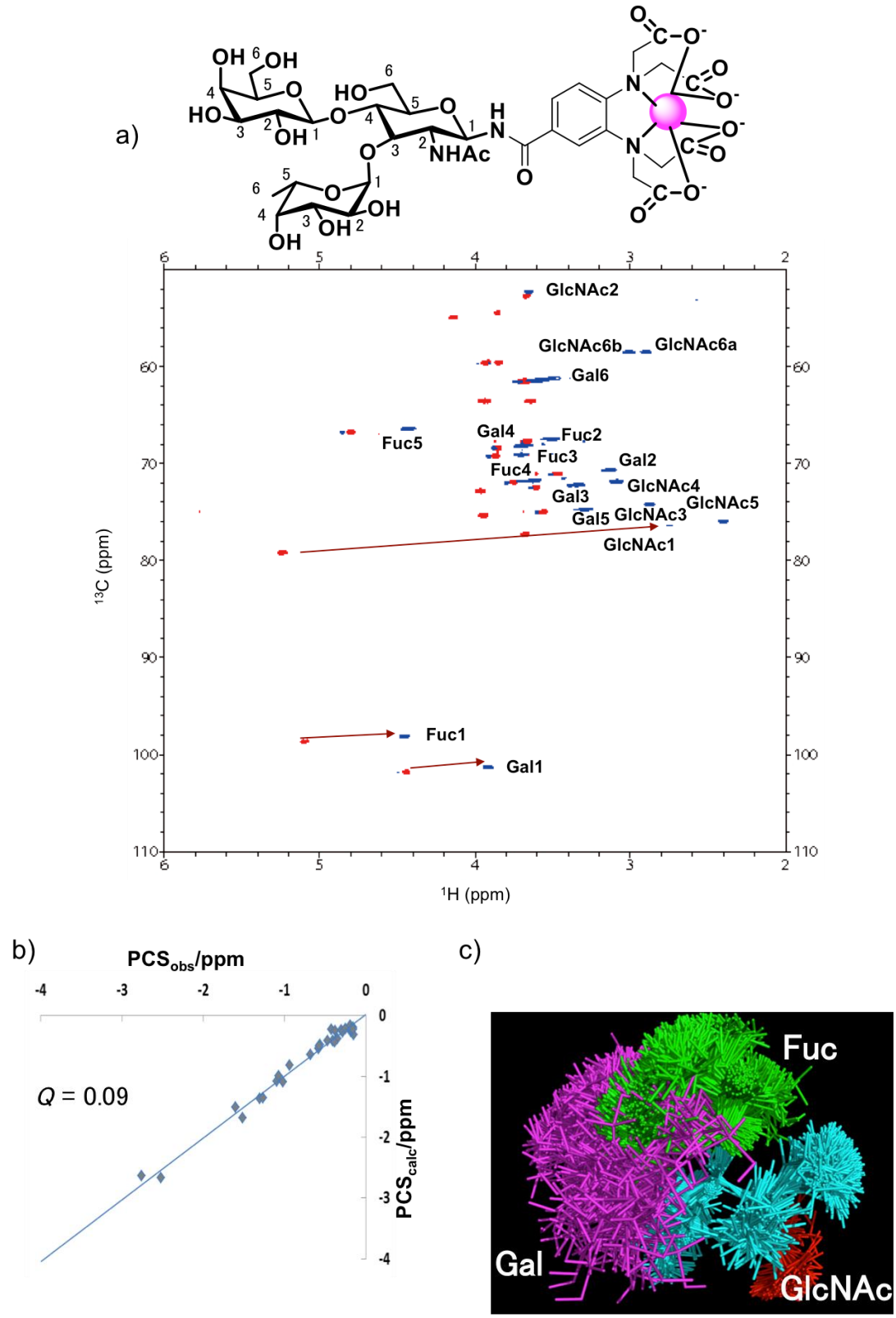

Figure 3. a) ^{1}H-^{13}C HSQC spectra of the Lewis X trisaccharide tagged with La^{3+} (red) and Tm^{3+} (blue) ions. b) Correlations between experimentally observed PCS values

and computationally calculated PCS data for the Lewis X trisaccharide. *Q* value, defined by the equation $Q = \mathrm{rms}(\mathrm{PCS_{calc}} - \mathrm{PCS_{obs}})/\mathrm{rms}(\mathrm{PCS_{obs}})$, is criteria of agreement between the experimental and calculated values. c) Conformational ensembles of Lewis X trisaccharide.

To gain insights into the Lewis X interaction with its cognate lectins, I inspected a reported crystal structure of AOL, a $_{L}$-fucose-specific lectin, complexed with fucose [15,16]. This lectin is known to be capable for binding to the Lewis X-carrying oligosaccharides [17]. Figure 4 shows the NMR-validated ensemble model of the Lewis X trisaccharide containing 265 simulated conformers superimposed on the crystal structure (PDB code: 5H47) of AOL in complex with fucose. Each conformer was extracted at equal intervals from the combined REMD trajectory and the fucose residue of the trisaccharide was superimposed on the ligand fucose in the complex. The model suggests the steric hindrance between the lectin and the Gal residue in the closed form of Lewis X. In contrast, the open conformations are accommodated in the carbohydrate-binding pocket without obvious steric crush. On the basis of the model, I suggest the conformational selection mechanism during the Lewis X recognition process by this lectin, raising the possibility that the lectin-binding affinity can be increased by elevating the open conformer population.

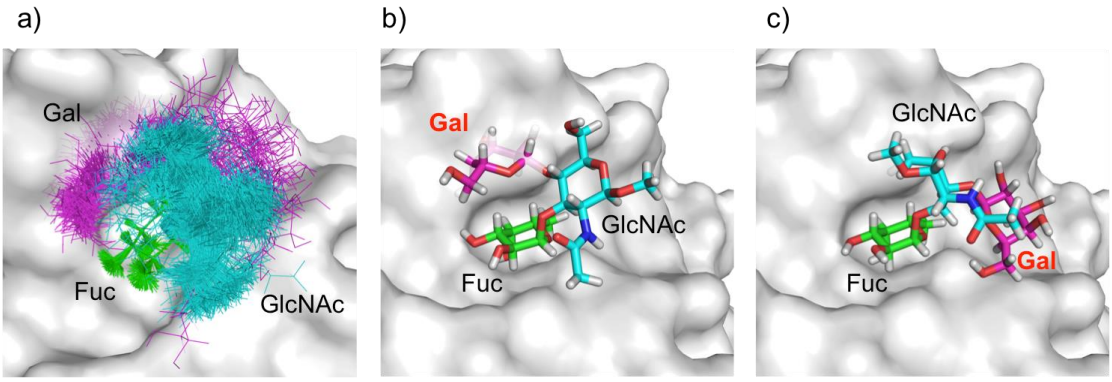

Figure 4. The surface model of AOL with a) the ensemble model, b) typical closed and c) open conformers of the Lewis X trisaccharide.

The closed conformation of the Lewis X trisaccharide is stabilized by the stacking between the Fuc and Gal residues with hydrogen bonding as well as steric restraint due to the bulky *N*-acetyl group of the GlcNAc residue [18,19]. Therefore, to examine the possibility, I designed and created Lewis X mimetics in an attempt to destabilize the closed conformation (Figure 5). By introducing stereoisomers, the hydrogen bonding involved in hydroxy groups in the Gal residue can be broken. Thus, I synthesized a Lewis X trisaccharide analogues **A**, Glcβ1-4(Fucα1-3)GlcNAc, in which the Glc residue as a stereoisomer of galactose was introduced. Another analogue **B**, Galβ1-4(Fucα1-3)Glc, exclusive of the NHAc group was also prepared to examine the impact of the bulky acetyl group of the GlcNAc residue. According to the superposed model, these modified groups are not directly involved in the lectin binding.

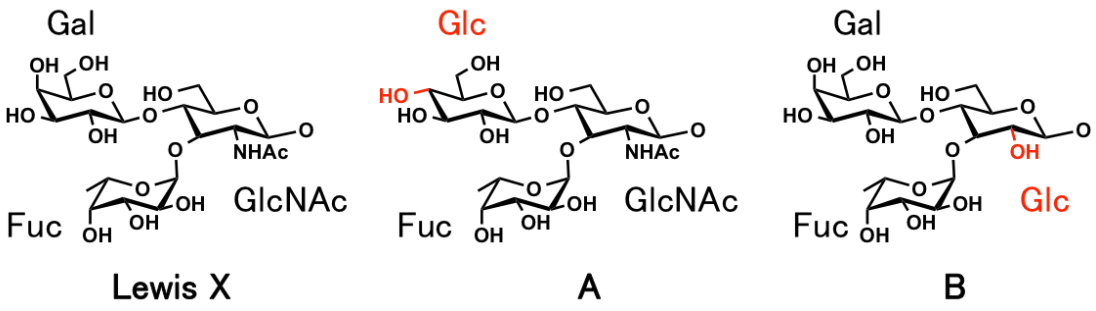

Figure 5. Representation of the structures of the Lewis X and its mimetics.

Using the lanthanide-tagging method, I acquired the experimental PCS data of these Lewis X analogues for validation of their conformational ensemble models generated by REMD simulations. On the basis of the experimentally validated simulations, I explored the conformational spaces occupied by these mimetic trisaccharides (Figures 6 and 7). The results revealed that the open conformations were more populated in the Lewis X mimetic **A** in comparison with the native Lewis X trisaccharide, while the conformational space of the mimetic **B** was little altered. These findings indicate that the hydrogen bonding between the Gal and Fuc residues is significantly contribute to stabilization of the closed conformation of the Lewis X trisaccharide.

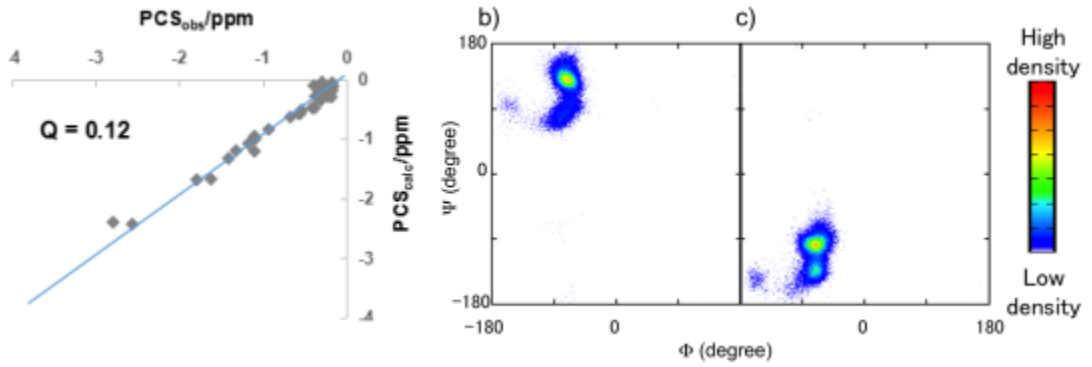

Figure 6. a) The correlations between experimentally observed PCS values and computationally calculated PCS data for the Lewis X mimetic A. b,c) Dihedral angles maps of the Glcβ1-4GlcNAc and c) the Fucα1-3GlcNAc, respectively.

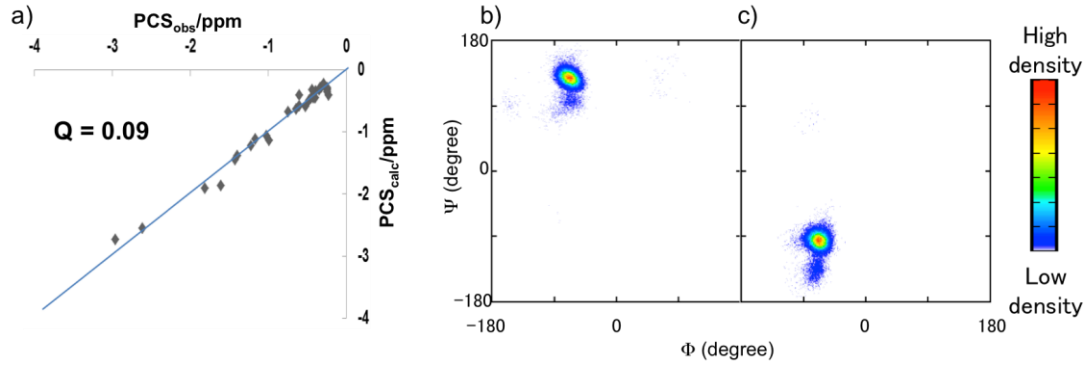

Figure 7. a) The correlations between experimentally observed PCS values and computationally calculated PCS data for the Lewis X mimetic B. b,c) Dihedral angles maps of the Galβ1-4Glc and c) the Fucα1-3Glc, respectively.

The lectin-binding affinity of the Lewis X trisaccharide with that of the mimetic **A** was compared by frontal affinity chromatographic (FAC) analyses [20,21]. The fluorescence-tagged trisaccharides were subjected to an AOL-immobilized column to estimate their affinities for the lectin by inspecting the retardation in elution (Figure 8).

The FAC data revealed that the mimetic **A** has a higher affinity for the lectin than that of the native Lewis X trisaccharide. Thus, I successfully increase the lectin-binding affinity of the oligosaccharide by tuning its conformation space.

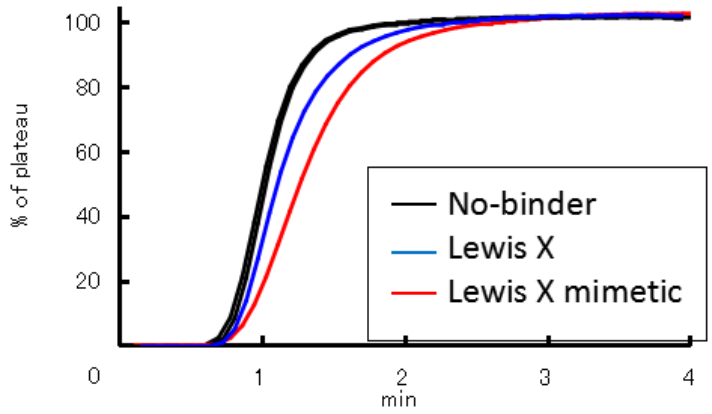

Figure 8. Elusion profiles of Galβ1-4GlcNAc disaccharide as a no-binder (black), the Lewis X trisaccharide (blue) and the mimetic A (red) on the AOL-immobilized column.

2.3 Conclusions

In this chapter, I applied the lanthanide-assisted NMR approach for characterizing the conformational dynamics of the Lewis X trisaccharide. The conformational space occupied by this trisaccharide was explored by the molecular simulation, which was successfully validated by inspecting the experimentally obtained PCS data. Moreover, the conformational space of the Lewis X trisaccharide was chemically remodeled, improving its binding affinity to the cognate lectin This success opens prospects for rational design of functional oligosaccharides, providing dynamic views of oligosaccharide-protein interactions.

2.4 Materials and Experiments

2.4.1 General

Lewis X-carrying oligosaccharides were chemically synthesized from glucosamine, fucose, glucose and galactose building blocks obtained from TCI Co. Solvents and reagents were also purchased from TCI Co., WAKO Pure Chemical Industries, KANTO Chemical Co., and Sigma-Aldrich Co. Column chromatography was performed using a Biotage Isolera medium-pressure liquid chromatography (MPLC) system with SNAP Ultra (for normal-phase chromatography) or SNAP Ultra C18 (for reversed-phase chromatography) columns, unless otherwise noted.

2.4.2 Molecular simulations of the oligosaccharides

The all atom REMD simulations of the Lewis X trisaccharide and its mimetics were performed by using AMBER14 program package [22]. The initial structures and topology files were created by employing the tLeap module of the AmberTools program. The GLYCAM06 force field was used for oligosaccharide [23]. TIP3P water models were added to the solvent layer to ensure a distance of at least 12 Å from any atom of the oligosaccharides and periodic boundary conditions were imposed. The unit time-step was 2.0 fs. Prior to performing the production runs, energy minimizations by the steepest-descent method were carried out, followed by 2.0 ns MD simulation at the *NPT* ensemble. All production REMD simulations were done at the *NVT* ensemble. REMD simulations were carried out for 53 ns with 64 replicates

(total simulation time, 3.3 μs) with an exponential temperature distribution between 300 and 500 K. Replica exchange was attempted every 1,000 steps. For analyzing the simulation results, the cpptraj module of the AmberTools program package was used.

2.4.3 Preparation of the tagged Lewis X trisaccharide

Suspended solution of compound **1** (1.36 g, 2.5 mmol), compound **2** (1.33 g, 2.7 mmol) and 3Å molecular sieves (2 g) in CH_2Cl_2 (8 mL) was stirred for 30 min at RT and subsequently cooled to -35 °C. Then TMSOTf (150 μL, 0.83 mmol) was added dropwise to the reaction mixture and stirred for 3 h at -35°C (completion of the reaction was confirmed by TLC analysis; EtOAc/Hexane, 1:1). The reaction mixture was neutralized by addition of saturated aqueous $NaHCO_3$ then filtered through celite. The filtrate was diluted with $CHCl_3$, and the organic phase was washed with saturated aqueous $NaHCO_3$, dried over Na_2SO_4, and concentrated. The residue was purified by SNAP Ultra normal phase column to give compound **3** (1.43 g, 65%).

Ammonium hexanitratocerate (IV) (3.51 g, 6.4 mmol) in H_2O (4 ml) was added dropwise to a solution of compound **3** (1.40 g, 1.6 mmol) in acetonitrile (12 ml) at 0°C. The reaction mixture was stirred for 30 min at 0°C (completion of the reaction was confirmed by TLC analysis; EtOAc/Hexane, 3:2). After dilution with EtOAc, the organic phase was washed with saturated aqueous $NaHCO_3$ and brine, dried over Na_2SO_4, and concentrated. The residue was purified by SNAP Ultra normal phase column to give compound **4** (785 mg, 64%).

Acetic anhydride (5 mL, 53 mmol) was added dropwise to a solution of

compound **4** (750 mg, 0.97 mmol) in pyridine (4 mL) in an ice-water bath. The reaction mixture was stirred for 10 h at room temperature (completion of the reaction was confirmed by TLC analysis; EtOAc/Hexane, 1:1). The reaction mixture was diluted with $CHCl_3$, and the organic phase was washed with 1_N aqueous HCl, saturated aqueous $NaHCO_3$ and brine, dried over Na_2SO_4 and concentrated. The residue was purified by SNAP Ultra normal phase column to give compound **5** (739 mg, 94%).

Trimethylsilyl azide (0.92 mL, 7.0 mmol) and $SnCl_4$ (430 μL, 3.7 mmol) were added to a solution of compound **5** (710 mg, 862 μmol) in CH_2Cl_2 (7 mL) at 0°C. The reaction mixture was stirred for 4 h at 0°C (completion of the reaction was confirmed by TLC analysis; EtOAc/Hexane, 3:2). The reaction mixture was diluted with $CHCl_3$, and the organic phase was washed with saturated aqueous $NaHCO_3$, H_2O, dried with Na_2SO_4, and concentrated. The residue was purified by SNAP Ultra normal phase column to give compound **6** (547 mg, 80%).

A mixture of $Ir(COD)(PMe_2Ph)_2PF_6$ (19 mg, 23 μmol) in THF (10 mL) was stirred at RT for 30 min under H_2 atmosphere, then the atmosphere was replaced by N_2. To the mixture of activated Ir complex in THF was added a solution of compound **6** (520 mg, 660 μmol) in THF (10 mL) under N_2 atmosphere, and stirred for 2 h at room temperature. After evaporation of THF, residue was suspended in 90% aqueous acetone (20 ml). Then to the reaction mixture, $HgCl_2$ (450 mg, 1.7 mmol) and HgO (57 mg, 220 μmol) were added and stirred for 2 h at RT (completion of the reaction was confirmed by TLC analysis; EtOAc/Hexane, 3:2). The reaction mixture was

diluted with $CHCl_3$, and the organic phase was washed with brine, dried over Na_2SO_4 and concentrated. The residue was purified by SNAP Ultra normal phase column to give compound **7** (400 mg, 80%).

Suspended solution of compound **7** (372 mg, 493 μmol), compound **8** (260 mg, 493 μmol), NIS (168 mg, 740 μmol) and 3Å molecular sieves (700 mg) in CH_2Cl_2 (5 mL) was stirred for 30min at RT and subsequently cooled to -40°C. Then TfOH (15 μL, 170 μmol) was added dropwise to the reaction mixture and stirred for 6 h at -40°C (completion of the reaction was confirmed by TLC analysis; EtOAc/Hexane, 1:1). The reaction mixture was neutralized by addition of saturated aqueous $NaHCO_3$ then filtered through celite. The filtrate was diluted with $CHCl_3$, and the organic phase was washed with 3% aqueous $Na_2S_2O_3$, saturated aqueous $NaHCO_3$, dried over Na_2SO_4, and concentrated. The residue was purified by SNAP Ultra normal phase column to give compound **9** (375 mg, 65%).

To a suspension of compound **9** (350 mg, 298 μmol) in 1-buthanol (4 mL), ethylenediamine (1 mL, 15 mmol) was added and the reaction mix was stirred for 18 h at 85°C. After cooling to room temperature, the reaction mixture was co-evaporated with toluene-CH_3OH and pumped in vacuo over 3 h. Then, the crude product was dissolved in pyridine (3 mL), and Ac_2O (1.5 mL, 15.9 mmol) was added dropwise to the solution in an ice-water bath. After stirring for 15 h at 50°C. The reaction mixture was cooled to room temperature and concentrated. The residue was diluted with EtOAc, and the organic phase was washed with 1_N aqueous HCl, H_2O, saturated aqueous $NaHCO_3$, brine, dried over Na_2SO_4, and concentrated. The residue was

roughly purified by SNAP Ultra normal phase column to give mixture of trisaccharides. The mixture of trisaccharides were dissolved in CH_3OH, and $Pd(OH)_2/C$ (80 mg) was added to the solution. The reaction mixture was stirred for 24 h at room temperature under an atmosphere of H_2 (completion of the reaction was confirmed by TLC analysis; $CH_3OH/CHCl_3$, 1:3). The reaction mixture was filtered through celite, concentrated, and purified by SNAP Ultra normal phase column to give compound **10** (118 mg, 57% in 3 steps).

Compound **11** (62 mg, 130 μmol), DMT-MM (35 mg, 130 μmol), and DIPEA (230 μL, 1.3 mmol) were dissolved in DMSO (5 mL) and the mixture was stirred for 10 min at room temperature. Subsequently, the mixture was transferred to a solution of compound **10** (83 mg, 120 μmol) in DMSO (1 mL), and stirred for 12 h at room temperature. (completion of the reaction was confirmed by TLC analysis; $CH_3OH/CHCl_3$, 1:3). The reaction mixture was diluted with EtOAc, and the organic phase was washed with H_2O, dried over Na_2SO_4, and concentrated. The residue was purified by SNAP Ultra normal phase column to give compound **12** (58 mg, 41%).

Compound **12** (43 mg, 37 μmol) was dissolved in CH_3OH and small aliquots of 1_M aqueous NaOH were added until the reaction was complete (completion of the reaction was confirmed by TLC analysis; $CH_3OH/CHCl_3/H_2O$, 5:5:1). The reaction mixture was purified by ODS column to give **13** (31 mg, 95%).

The Lewis X mimetics **A** and **B** were synthesized following the similar protocols as shown in Schemes 2 and 3, respectively.

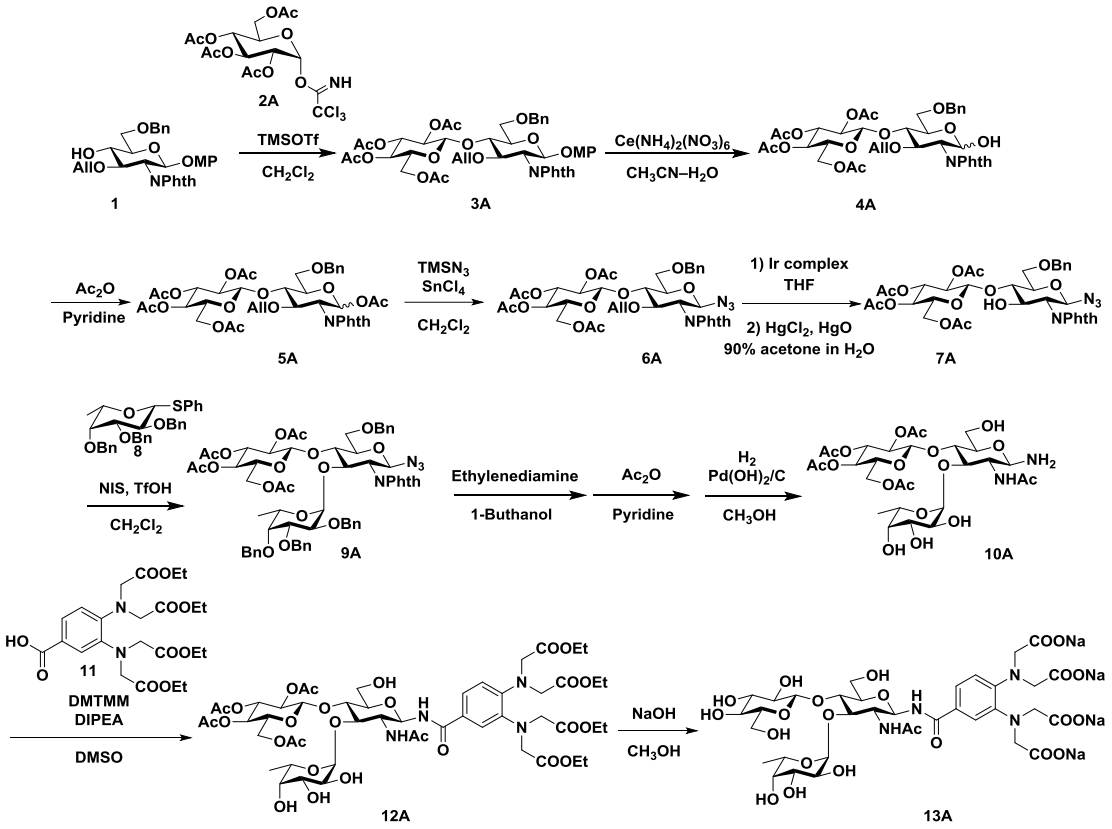

Scheme 2. Synthesis of the Lewis X mimetic **A** tagged with the lanthanide-chelating unit.

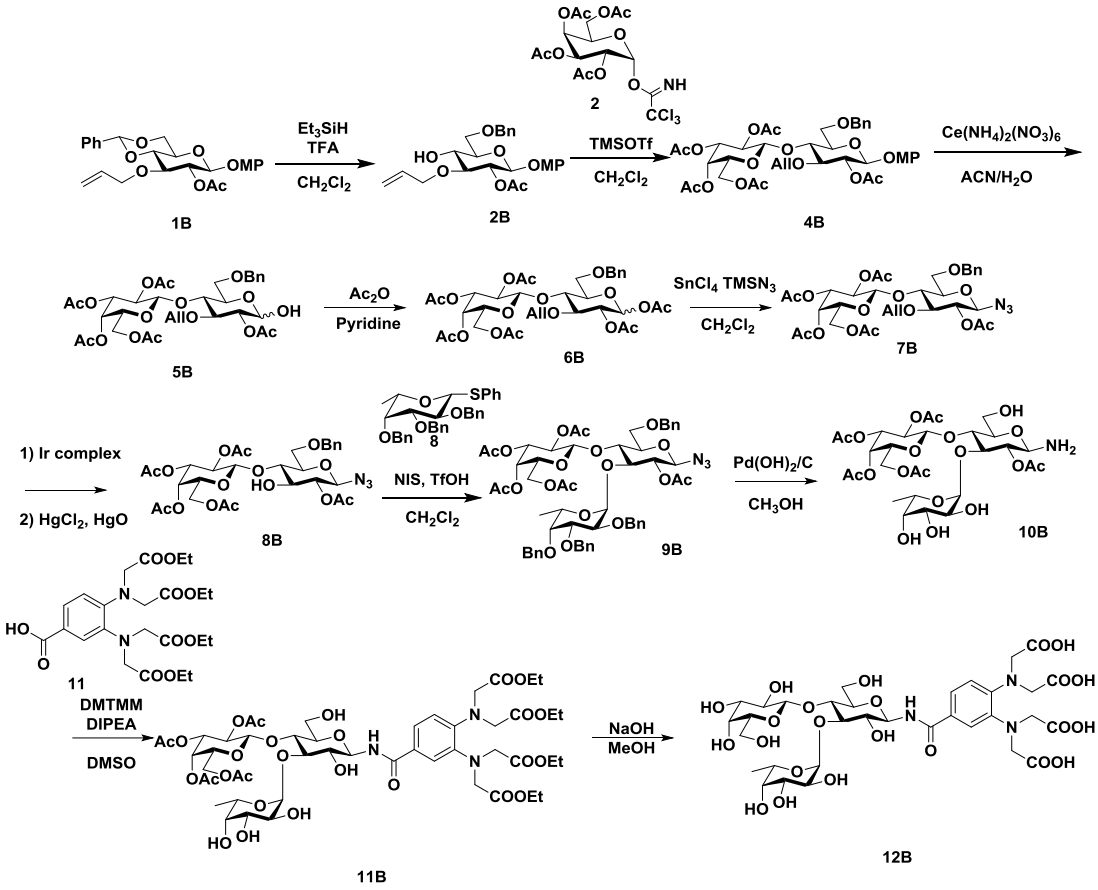

Scheme 3. Synthesis of the Lewis X mimetic **B** tagged with the lanthanide-chelating unit.

2.4.4 PCS measurements and analyses

The tagged trisaccharide was dissolved in D_2O and adjusted to pH 8.0 with NaOD to stabilize the complex. This solution was titrated with MCl_3 in D_2O (250 mM; M= La^{3+} or Tm^{3+}) for NMR. For the PCS observation, NMR spectra were obtained at 300 K in an Avance 800 spectrometer (Bruker) equipped with a cryoprobe at the Instrument Center in IMS. ^{1}H-^{13}C HSQC spectra were recorded at a proton observation frequency of 800.3 MHz with 256 (t_1) and 2,048 (t_2) complex points. NMR spectra were processed and analyzed in TopSpin (v2.1, Bruker) and SPARKY

(T.D. Goddard and D.G. Kneller, SPARKY 3, University of California, San Francisco).

From the combined REMD trajectories of the oligosaccharide, 26,500 conformers were extracted at equal intervals, and the calculated average position of the paramagnetic center relative to the reducing-terminal GlcNAc or Glc residue of the trisaccharide was positioned in the ensemble model. Subsequently, the $\Delta\chi$ tensor for the ensemble of 26,500 conformers incorporating the paramagnetic ion was estimated by a modified version of MSpin software (http://mestrelab.com/). A single $\Delta\chi$ tensor was determined for the conformational ensemble of each trisaccharide from the experimentally obtained PCSs, with the assumption that every conformer contributed equally to the PCSs, thereby providing the back-calculated PCS values of the oligosaccharide with Tm^{3+}.

2.4.5 FAC Analyses

The fluorescein-tagged Le X and the mimetic trisaccharides for the FAC analyses were synthesized as shown in Scheme 4.

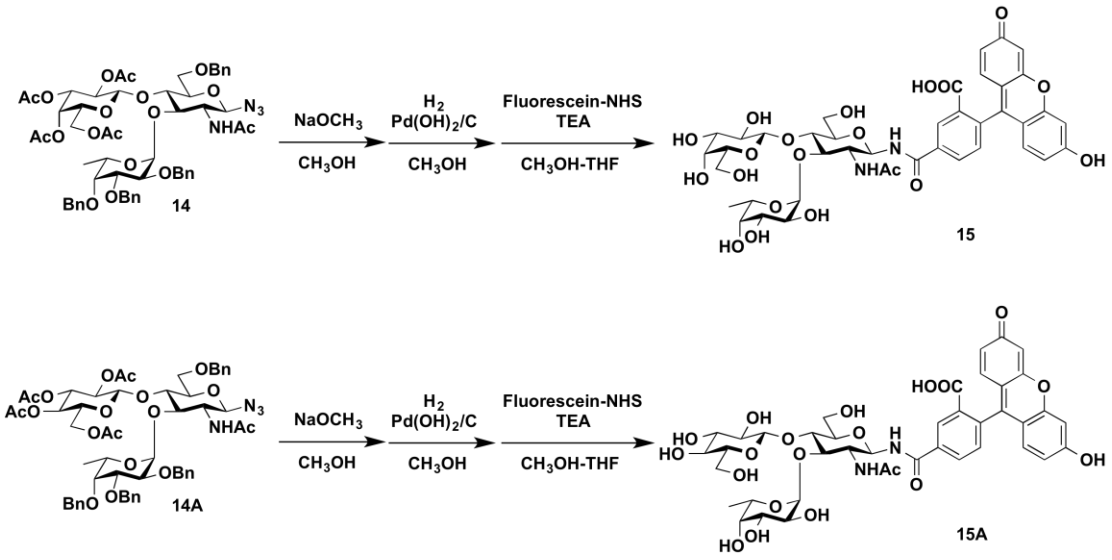

Scheme 4. Synthesis of the fluorescein-tagged trisaccharides.

To a solution of compound **14** (12 mg, 11 μmol) in CH_3OH (540 μl), 1_N $NaOCH_3$ in CH_3OH (11 μl, 11 μmol) was added at room temperature. Reaction mixture was stirred for 3.5 h at room temperature (completion of the reaction was confirmed by TLC analysis; $CH_3OH/CHCl_3$, 1:10) then neutralized with Dowex50Wx4 resin (H^+ form), filtered off, concentrated and pumped *in vacuo* over 3 h. Then the crude product was dissolved in CH_3OH and added $Pd(OH)_2/C$ (10 mg) was added at room temperature. The reaction mixture was stirred for 20 h at room temperature under atmosphere of H_2 and added another amount of $Pd(OH)_2/C$ (10 mg). The reaction mixture was stirred for totally 43 h (completion of the reaction was confirmed by TLC analysis; $CH_3OH/CHCl_3$, 1:5), filtered through celite, concentrated and pumped *in vacuo* over 3 h. Then, the crude product was dissolved in CH_3OH-THF = 1:1 (1.1 ml) and added triethylamine (3 μl, 22 μmol) and fluorescein *N*-hydroxysuccinimide ester (15 mg, 32 μmol) at room temperature. Reaction mixture was stirred for 30 h at room

temperature under dark condition then added another amount of triethylamine (3 μl, 22 μmol). The reaction mixture was stirred for totally 57 h (completion of the reaction was confirmed by TLC analysis; $CH_3OH/CHCl_3$, 1:5) and concentrated. The crude product was purified by HPLC (SHIMADZU HRC-ODS column, H_2O-CH_3CN gradient system) to obtain compound **15**. Compound **15A** was also prepared following the similar protocol. The fluorescein-tagged trisaccharides were subjected to FAC analyses.

References:

1. K. Drickamer, ME. Taylor, Annu Rev Cell Biol. 1993, 9, 237–264.

2. N. Sharon and H. Lis, Lectins, 2nd edn. Springer, Dordrecht, 2003.

3. G. Kozlov, C.L. Pocanschi, A. Rosenauer, S. Bastos-Aristizabal, A. Gorelik, D.B. Williams and K. Gehring, J Biol Chem. 2010, 285, 38612–38620.

4. T. Satoh, N.P. Cowieson, W. Hakamata, H. Ideo, K. Fukushima, M. Kurihara, R. Kato, K. Yamashita and S. Wakatsuki. J Biol Chem. 2007, 282, 28246–28255.

5. S. Perez, N. Mouhous-Riou, N. E. Nifantev, Y. E. Tsvetkov, B. Bachet and A. Imberty, Glycobiology. 1996, 6, 537-542.

6. H. F. Azurmendi, M. Martin-Pastor and C. A. Bush, Biopolymers. 2002, 63, 89-98.

7. J. Topin, M. Lelimousin, J. Arnaud, A. Audfray, S. Perez, A. Varrot and A. Imberty, ACS Chem. Biol. 2016, 11, 2011-2020.

8. Y. Sugita, Y. Okamoto, Chem. Phys. Lett. 1999, 314, 141-151.

9. S. Re, W. Nishima, N. Miyashita, Y. Sugita, Biophys. Rev. 2012, 4, 179-187.

10. S. Pérez, N. Mouhous-Riou, N. E. Nifant'ev, Y. E. Tsvetkov, B. Bachet, A. Imberty, Glycobiology 1996, 6, 537-542.

11. T. Yamaguchi, Y. Sakae, Y. Zhang, S. Yamamoto, Y. Okamoto, K. Kato, Angew Chem Int Ed 2014, 53, 10941-10944.

12. T. Suzuki, M. Kajino, S. Yanaka, T. Zhu, H. Yagi, T. Satoh, T. Yamaguchi, K. Kato, ChemBioChem 2017, 18, 396-401.

13. G. Otting, Annu. Rev. Biophys. 2010, 39, 387-405.

14. T. Yamaguchi and K. Kato, Glycoscience: Biology and Medicine, Springer (Japan), 2014, vol.1, pp.137-145.

15. H. Makyio, J. Shimabukuro, T. Suzuki, A. Imamura, H. Ishida, M. Kiso, H. Ando, R. Kato, Biochem Biophys Res Commun. 2016, 477, 477-482.

16. J. Shimabukuro, H. Makyio, T. Suzuki, Y. Nishikawa, M. Kawasaki, A. Imamura, H. Ishida, H. Ando, R. Kato, M. Kiso, Bioorg. Med. Chem., 2017, 25, 1132-1142.

17. K. Matsumura, K. Higashida, H. Ishida, Y. Hata, K. Yamamoto, M. Shigeta, Y. Mizuno-Horikawa, X. Wang, E. Miyoshi, J. Gu, N. Taniguchi, J Biol Chem. 2007, 282, 15700-15708.

18. M. Zierke, M. Smieško, S. Rabbani, T. Aeschbacher, B. Cutting, F. H.-T. Allain, M. Schubert, B. Ernst, J. Am. Chem. Soc., 2013, 135, 13464-13472.

19. M. D. Battistel, H. F. Azurmendi, M. Frank, D. I. Freedberg, J Am Chem Soc. 2015, 137, 3444-3447.

20. K. Kasai, Y. Oda, M. Nishikawa, S. Ishii, J. Chromatogr. 1986, 376, 33-47.

21. J. Hirabayashi, Y. Arata, K. Kasai, MethodsEnzymol. 2003, 362, 353-368.

22. D. A. Case, T. E. Cheatham, T. Darden, H. Gohlke, R. Luo, K. M. Merz, A. Onufriev, C. Simmerling, B. Wang, R. J. Woods, J Comput Chem 2005, 26, 1668-1688.

23. K. N. Kirschner, A. B. Yongye, S. M. Tschampel, J. Gonzalez-Outeirino, C. R. Daniels, B. L. Foley, R. J. Woods, J. Comput. Chem. 2008, 29, 622-655.

Chapter 3: NMR analysis of Ca^{2+}-mediated carbohydrate-carbohydrate interactions between Lewis X clusters

This chapter is adapted and modified from Gengwei Yan, Takumi Yamaguchi, Tatsuya Suzuki, Saeko Yanaka, Sota Sato, Makoto Fujita, and Koichi Kato, "Hyper-Assembly of Self-Assembled Glycoclusters Mediated by Specific Carbohydrate–Carbohydrate Interactions," Chem. Asian J. 2017, 12, 968-972. DOI: 10.1002/asia.201700202

3.1 Introduction

Oligosaccharides form clusters on viral and cellular surfaces and play pivotal roles in various physiological and pathological processes, including infections and cell adhesion through carbohydrate–protein and carbohydrate–carbohydrate interactions [1-3]. The affinities of the carbohydrates involved in these interactions are very weak but are avidly enhanced by the multivalent binding achieved by their clustering [4-6]. In particular, the importance of carbohydrate–carbohydrate interactions in their clustered states has been widely recognized in cell–cell interactions [7-8].

For a better understanding of the functional mechanisms relevant to oligosaccharides on cell membranes, it is desirable to develop appropriate models of their clusters [9-12]. For characterizing carbohydrate–carbohydrate interactions, various glycoclusters have been fabricated by accumulation of carbohydrates on artificial scaffolds such as polymers, nanoparticles, and liposomes, and characterized using analytical techniques such as transmission electron microscopy, atomic force microscopy and surface plasmon resonance measurements [13-23]. However, the physicochemical and structural properties of carbohydrate clusters remain largely unknown, primarily because of the lack of an appropriate glycocluster model system that combines structural homogeneity and the functional ability to promote carbohydrate–carbohydrate interactions.

In this chapter, I created Lewis X-carrying glycoclusters by hybridizing self-assembled metal-organic complexes with the synthetic carbohydrate moieties as structurally well-defined oligosaccharide clusters for NMR characterization of carbohydrate-carbohydrate interactions. It has been supposed that Lewis X clusters on cell surfaces can mediate cell–cell interactions through their Ca^{2+}-mediated homophilic bindings [24-28].

A series of self-assembled, spherical complexes composed of Pd^{2+} ions (M) and organic ligands (L) can define stable and discrete interfaces and spaces [29,30], thereby providing unique reaction stages, as demonstrated by their application in the templated synthesis of silica nanoparticles [31]. These complexes also offer structural scaffolds for functional biomimetic systems, as exemplified by protein encapsulation within the complex [32]. Furthermore, the self-assembled spherical complexes can display carbohydrate moieties and thereby exhibit specific interactions with lectins such as concanavalin A and peanut agglutinin [33]. In addition to these stoichiometric carbohydrate–protein interactions, the spherical complexes could also be endowed with the ability to capture amyloidogenic proteins such as amyloid β and α-synuclein by modifying their surface through transplantation of a pentasaccharide derived from ganglioside GM1 [34], a glycosphingolipid abundant in neural cell membranes, so as to form a continuous surface covered by the glycans for affinity enhancement [35]. Thus I attempted to extend the applicability of this

molecular hybrid approach to create a carbohydrate–carbohydrate interaction system.

3.2 Results and Discussion

To develop bidentate ligand **1,** which harbors a Lewis X derivative as a functional *glycotope*, the chemically synthesized Lewis X trisaccharide was covalently linked to a bent unit through a disaccharide spacer. The structure of ligand **1a** was characterized by solution NMR spectroscopy and high-resolution mass spectrometry. The self-assembly of a Lewis X-carrying glycocluster **2a** from ligand **1a** and Pd^{2+} ion was achieved based on a previous report [34] with modifications (Figure 1). Ligand **1a** (1.6 μmol) was treated with $Pd(NO_3)_2$ (0.9 μmol) in DMSO for 12 h. The reaction mixture was subjected to a desalting column and dialyzed against D_2O to remove excess Pd^{2+} ions and DMSO.

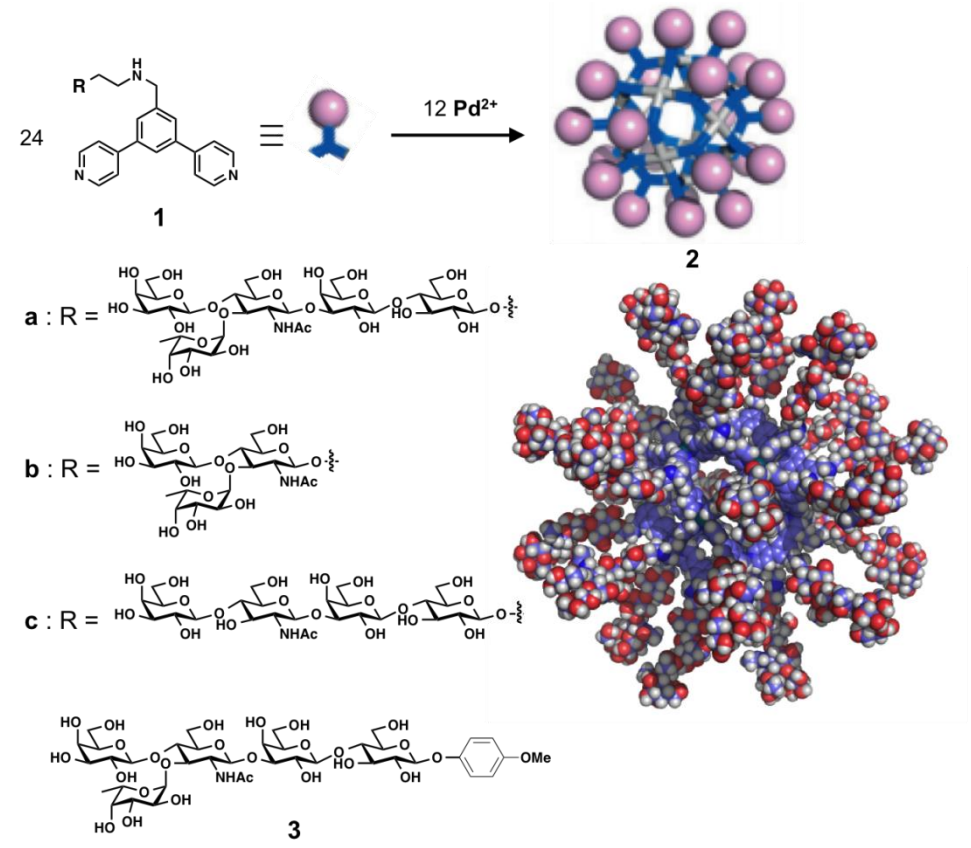

Figure 1. Self-assembly of glycocluster **2** from Pd^{2+} ions and bidentate ligand **1** bearing Lewis X sugar. The molecular structure of **2a** was optimized by MM calculation (Pd: green, C: light blue, N: blue, O: red, H: gray).

The selective formation of spherical complex **2a** was observed by ^{1}H NMR measurement of the D_2O solution, in which the signals were broadened due to the large complex formation (Figure 2). A downfield shift ($\Delta\delta$ = 0.37 ppm) of the signals at the pyridyl α-positions indicated the formation of coordination bonds between the pyridyl groups and Pd^{2+} ions. The large spherical structure with a uniform size was also confirmed by diffusion-ordered spectroscopy (DOSY) measurements of the complex (observed diffusion coefficient D = 6.8×10^{-11} m^2 s^{-1}) compared with its component **1a** (D =

2.2×10^{-10} m^2 s^{-1}) (Figure 2). Molecular mechanics (MM) calculation indicated that the self-assembled glycocluster **2a** accumulated 24 Lewis X sugar moieties on the periphery of an $M_{12}L_{24}$ spherical complex with a maximum diameter of 8 nm (Figure 1).

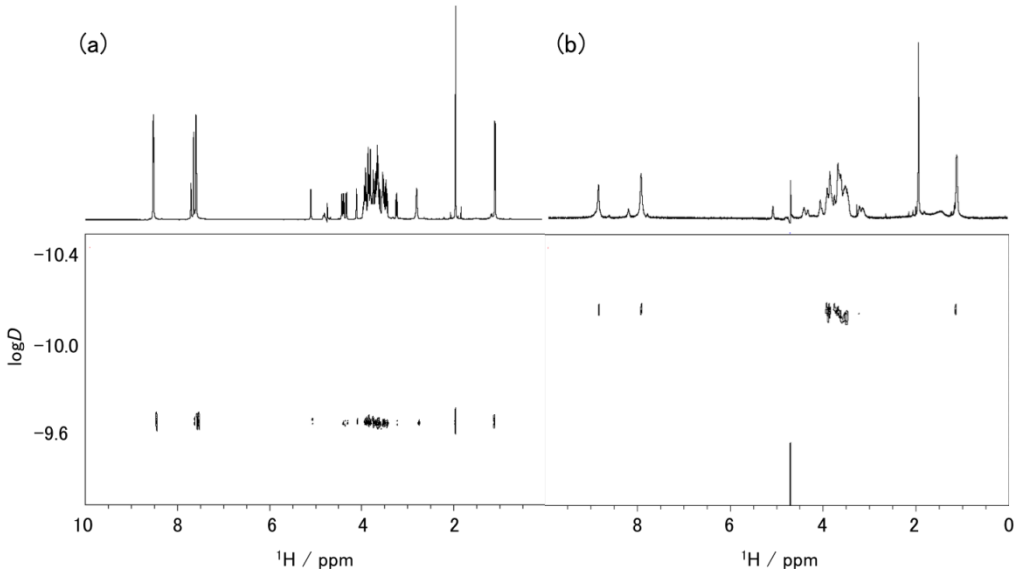

Figure 2. ^{1}H NMR and DOSY spectra of (a) ligand **1a** and (b) glycocluster **2a**.

To examine possible interactions between the glycoclusters in water, dynamic light scattering (DLS) measurements were performed with complex **2a** before and after adding Ca^{2+} ions (Figure 3). The observed DLS peaks from the self-assembled glcycocluster **2a** correspond to hydrodynamic radii of ca. 2 nm, which are smaller than the simulated diameter, presumably due to the hollow spherical structure. Upon addition of $CaCl_2$ (150 mM), larger particles were observed, indicating assembly of complex **2a** through Ca^{2+}-dependent Lewis X–Lewis X interactions. The aggregation was reversibly disassembled upon removal of Ca^{2+} ions by dialysis (Figure 4). Moreover, the diffusion coefficient

of complex **2a** decreased in the presence of Ca^{2+} in DOSY observations in D_2O, also indicating homophilic hyper-assembly of the spherical clusters. In contrast, DOSY measurements of monomeric **1a** with Ca^{2+} ions showed no change in its diffusion coefficient, confirming that cluster formation is a prerequisite for the Lewis X-mediated intermolecular interaction (Figure 5).

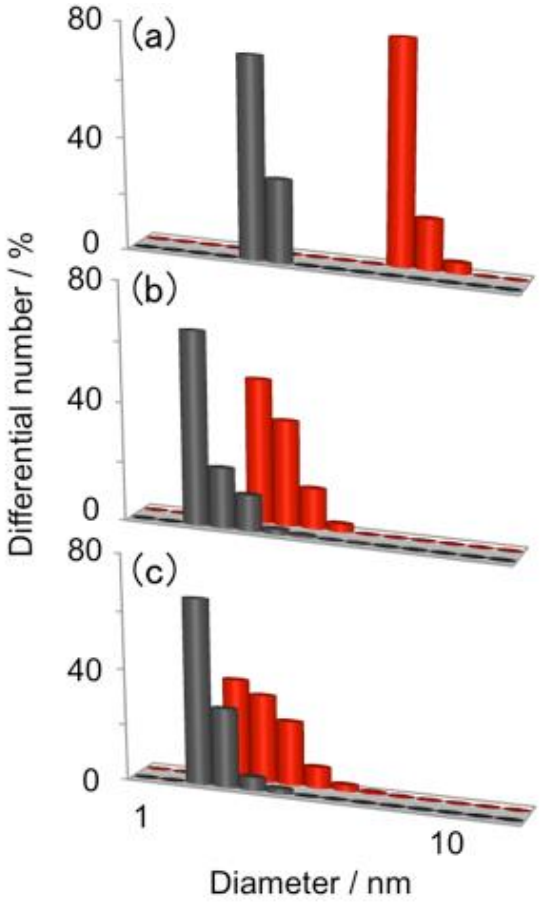

Figure 3. Size distributions observed in DLS measurements of (a) self-assembled glycoclusters **2a**, (b) **2b,** and (c) **2c** (0.2 mM each) before (black) and after (red) addition of Ca^{2+} ions (150 mM, 30 equiv. of the sugar unit).

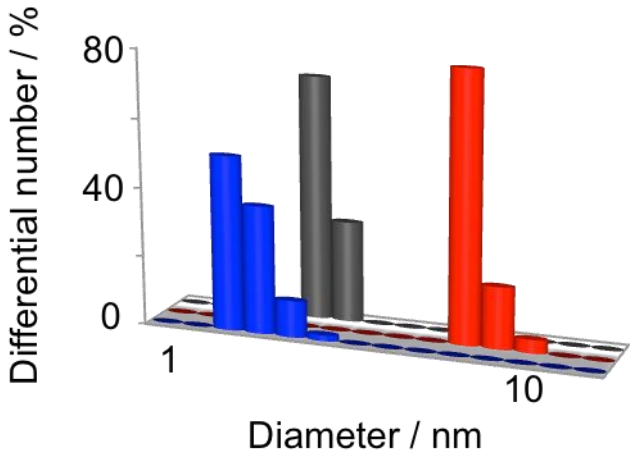

Figure 4. Size distributions observed in DLS measurements of glycocluster **2a** before (black) and after (red) addition of 150 mM Ca^{2+} and that observed after removal of Ca^{2+} by dialysis (blue).

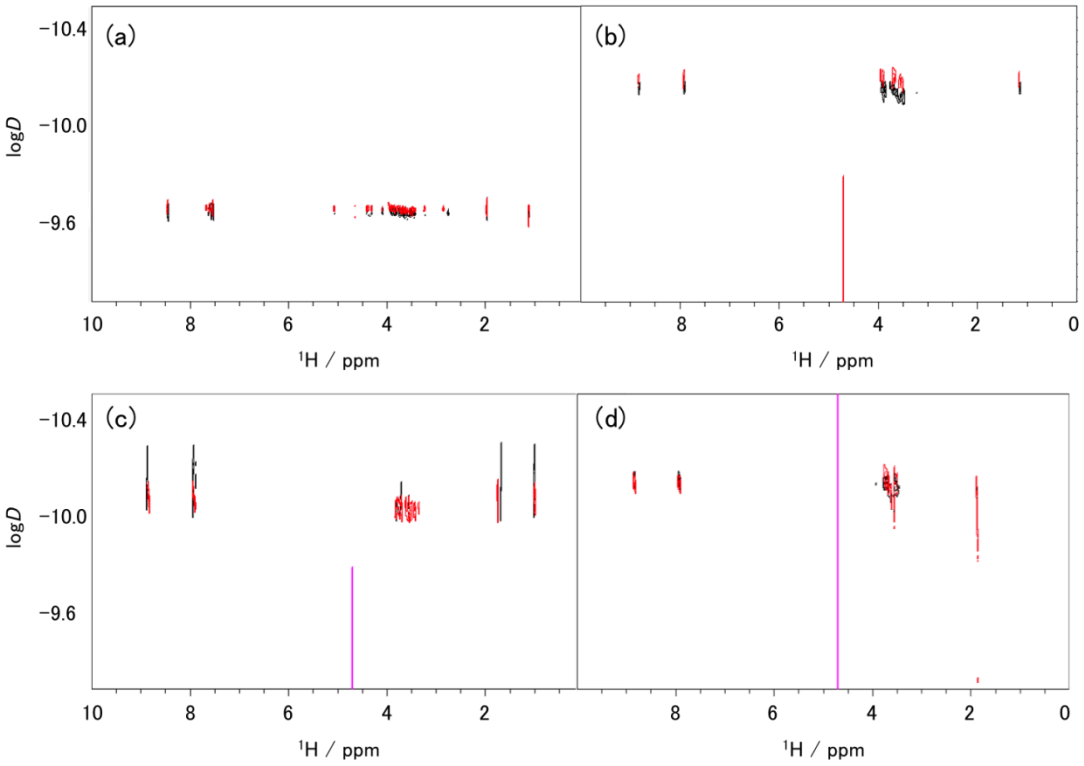

Figure 5. DOSY spectra of (a) ligand **1a,** (b) glycocluster **2a**, (c) **2b**, and (d) **2c** with (red) and without (black) Ca^{2+} ions.

The DLS and DOSY data also indicated that glycoclusters **2b** and **2c**, which assembled from bidentate ligands **1b** and **1c**, respectively, underwent no hyper-assembly, even in the presence of 150 mM Ca^{2+}, indicating that the removal of the spacer unit or the fucose residue from the Lewis X-carrying ligand impaired the observed carbohydrate-carbohydrate interactions (Figure 3 and 5). ^{1}H-^{13}C HSQC spectra confirmed that glycocluster **2a** but not **2b**, showed significant chemical shift changes upon addition of 150 mM Ca^{2+} (Fugures 6 and 7). These results suggest that not only the outer determinant but also the inner linker is important for the Ca^{2+}-dependent inter-cluster carbohydrate interactions.

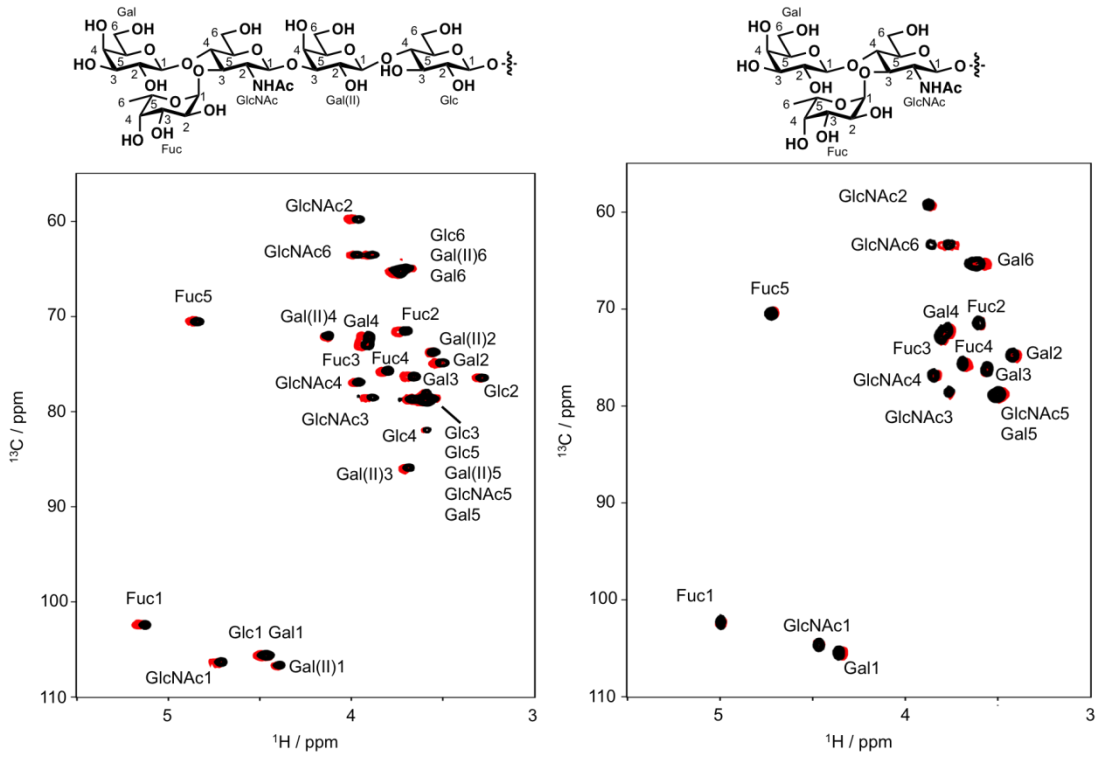

Figure 6. ^{1}H-^{13}C HSQC spectra of glycoclusters (a) **2a** and (b) **2b** before (black) and after (red) addition of 150 mM Ca^{2+}

Figure 7. The proton chemical shift perturbation values of **2a** (green) and **2b** (orange) upon addition of 150 mM Ca^{2+}. Asterisks indicate overlapping peaks.

The well-defined architecture of the spherical complex with a uniform nanoscale size will be suitable for detailed characterization of the glycan-mediated molecular process by solution NMR spectroscopy. I attempted to identify Ca^{2+}-binding site on the carbohydrate moieties of glycocluster **2a** based on NMR data. However, Ca^{2+} induced chemical shift perturbation for each CH group in a non-specific manner, probably because the observed chemical shifts were ascribed to not only the metal binding but also the consequent hyper-assembly mediated through carbohydrate-carbohydrate interactions.

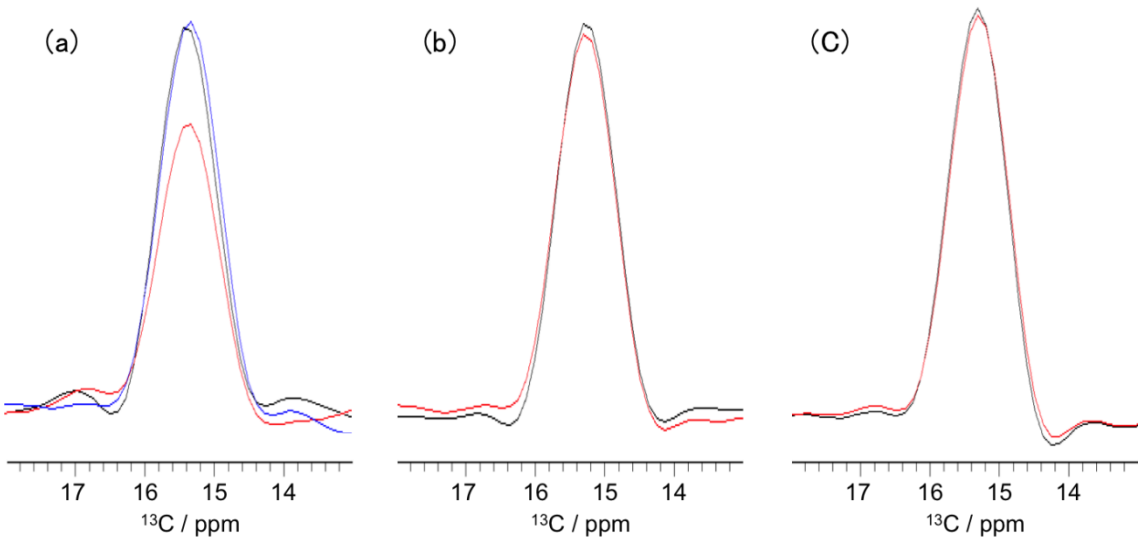

Figure 8. One-dimensional slices along the ω_1 dimension of HSQC spectra at the peak top position of the Fuc methyl group of glycoclusters (a) **2a** and (b) **2b** (0.04 mM each) and (c) monomeric Lewis X sugar derivative **3** (1mM) in the absence (black) and presence of 1 mM Mn^{2+} (red). In a, the result of competition experiment is shown in the presence of 1 mM Mn^{2+} and 5 mM Ca^{2+} (blue).

Hence, I employed paramagnetic effects, which are generally more sensitive and selective than chemical shift perturbation [36]. In the presence of Mn^{2+} (1 mM), glycocluster **2a** (0.04 mM) exhibited attenuation of peak intensity as exemplified by the Fuc methyl peak due to paramagnetic relaxation enhancement (PRE) (Figure 8a). The peak intensity was recovered by further addition of Ca^{2+} (5 mM), indicating that Mn^{2+} and Ca^{2+} compete with each other for the same binding site (Figure 8a). Moreover, Mn^{2+}-induced PRE was not observed for glycocluster **2b** and a monomeric Lewis X sugar **3** (Figure 8b and 8c). All these data indicate that Mn^{2+} serves as a useful paramagnetic probe to identify the Ca^{2+}-binding site of glycocluster **2a**. The observed PRE effects

are mapped on the carbohydrate moiety of **2a**, suggesting that not only the Lewis X trisaccharide but also the inner galactose residue contributes to Ca^{2+} binding (Figure 9). This is consistent with the observation that the inner lactose unit is indispensable for the Ca^{2+}-mediated hyperassembly (Figure 3 and 5). Although metal binding to the corresponding galactose residue has been observed for a free form of this pentasaccharide in organic solvent [37], glycocluster formation is essential for the observed metal binding in an aqueous environment.

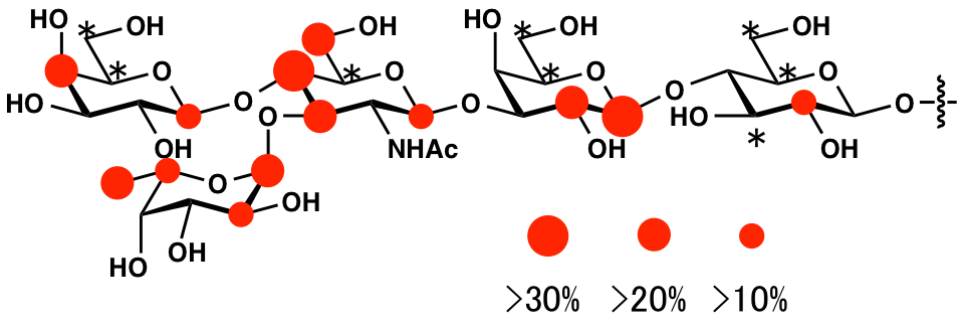

Figure 9. Mapping of attenuation of the CH peak intensity upon addition of Mn^{2+} on the CH groups of the Lewis X sugar moiety of glycocluster **2a**. Asterisks indicate overlapping peaks.

3.3 Conclusions

In this chapter, I successfully created a self-assembled, Lewis X-carrying glycocluster by hybridizing a spherical metal-organic complex with a synthesized oligosaccharide derivative. The glycocluster, which accumulates 24 Lewis X sugar moieties on its scaffold, exhibited Ca^{2+}-mediated homophilic

hyper-assembly, as demonstrated by DLS and NMR measurements. The facile preparation of this well-defined model of oligosaccharide clusters enables detailed structural characterization of the carbohydrate-mediated interactions at the atomic level using solution NMR spectroscopy and other physicochemical and biophysical techniques, thereby offering a useful tool for understanding the functional mechanisms of carbohydrate clusters. Moreover, this approach by hybridizing biomolecules and artificial supramolecules will provide a structural platform for designing and creating cyborg glycoclusters having unique functionality combining cell recognition and biomolecular encapsulation capabilities.

3.4 Materials and Experiments

3.4.1 General

Lewis X-carrying oligosaccharides were chemically synthesized from glucosamine, fucose, galactose, and lactose building blocks obtained from TCI Co. Solvents and reagents were also purchased from TCI Co., WAKO Pure Chemical Industries, KANTO Chemical Co., and Sigma-Aldrich Co.

Column chromatography was performed using a Biotage Isolera medium-pressure liquid chromatography (MPLC) system with SNAP Ultra (for normal-phase chromatography) or SNAP Ultra C18 (for reversed-phase chromatography) columns. High-resolution mass spectra (HRMS) were recorded on a

Bruker SolariX mass spectrometer (at the Center for Nano Materials and Technology, JAIST).

NMR spectra were recorded on a Bruker Avance III 500 spectrometer equipped with a cryoprobe. All the NMR spectral data were collected at 300 K. The chemical shift values are reported with respect to an external 4,4-dimethyl-4-silapentane-1-sulfonic acid standard. NMR spectra were processed and analyzed using the Bruker TopSpin 3.5 software and SPARKY (T.D. Goddard and D.G. Kneller, SPARKY 3, University of California, San Francisco). Dynamic light scattering (DLS) measurements were performed by an OTSUKA Electronics ELSZ-1000 particle analyzer at room temperature.

Molecular mechanics calculation was performed using the Forcite module of the Accelrys Materials Studio software suite. The geometrical optimization was carried out using the Universal force field and the charge calculation was performed using a QEq value of 1.1.

3.4.2 Preparation of ligand

Scheme 1. Synthesis of Lewis X-carrying ligand **1a**.

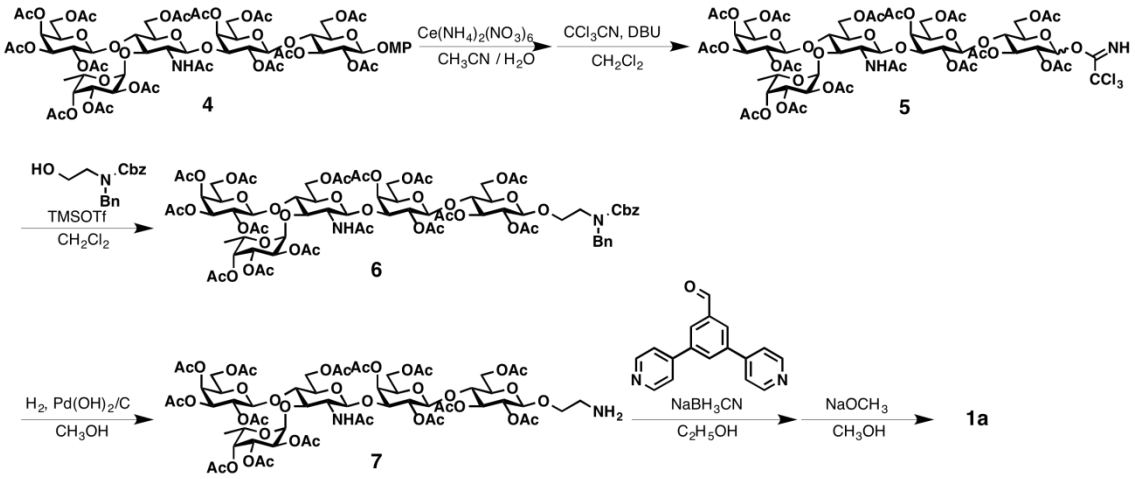

Lewis X-carrying ligand **1a** was synthesized as shown in Scheme 1. Ammonium cerium(IV) nitrate (2.83 g, 5.16 mmol) in water (8 ml) was added dropwise to an acetonitrile solution (24 ml) of Lewis X-carrying pentasaccharide **4** (2.0 g, 1.29 mmol) in an ice/water bath and the mixture was stirred for 0.5 h at 0 °C. After dilution with EtOAc, the organic phase was washed with saturated $NaHCO_3$ aq. and brine and dried over Na_2SO_4. The organic layer was concentrated in vacuo and fractionated by MPLC on a normal-phase column ($CHCl_3$/CH_3OH). Subsequently, the pentasaccharide derivative was converted to imidate **5** by treating it with trichloroacetonitrile. A mixture of the pentasaccharide derivative (1.57 g, 1.09 mmol), trichloroacetonitrile (1.1 ml, 10.9 mmol), and a catalytic amount of 1,8-diazabicyclo[5.4.0]undec-7-ene in dehydrated dichloromethane (15 ml) was stirred for 3 h at room temperature under an atmosphere of nitrogen. After concentrating the mixture in vacuo, the residue was

fractionated by MPLC with a normal-phase column ($CHCl_3/CH_3OH$) to give **5** as a mixture of anomers (1.5 g, 74% in 2 steps), which was linked with benzyl benzyl(2-hydroxyethyl)carbamate. A solution of the imidate (1.3 g, 0.83 mmol) and benzyl benzyl(2-hydroxyethyl)carbamate (260 mg, 0.91 mmol) in dehydrated dichloromethane (10 mL) containing MS 3 Å (3 g) was stirred at room temperature for 0.5 h and trimethylsilyl triflate (150 μL) was added into the solution at −40 °C. After the reaction mixture was stirred for 10 h at −40 °C under an atmosphere of nitrogen, the solution diluted by adding $CHCl_3$ was washed with saturated $NaHCO_3$ aq. and brine and dried over Na_2SO_4. The organic layer was concentrated in vacuo and purified by MPLC on a silica-gel column ($CHCl_3/CH_3OH$) to give compound **6** (830 mg, 58%).

The deprotection of **6** was achieved by catalytic reduction. A mixture of **6** (100 mg, 58 μmol) and $Pd(OH)_2/C$ in CH_3OH was stirred for 2 h at room temperature under an atmosphere of hydrogen. After completion of the reaction, the mixture was filtered through celite and the filtrate was concentrated. The obtained compound **7** was used without further purification for the reductive amination reaction. The pentasaccharide derivative **7** (75 mg, 51 μmol) and 3,5-bis(4-pyridyl)benzaldehyde (20 mg, 79 μmol) were mixed in dehydrated ethanol (10 mL) at 50 °C for 1 h under an atmosphere of nitrogen. Sodium cyanoborohydride (2.1 mg, 51 μmol) in CH_3OH (0.5 mL) was added, and the solution was stirred at 50 °C for 3 h. After the solution was evaporated in vacuo, the residue was loaded on a silica-gel column and eluted with $EtOAc/CH_3OH/H_2O$ to collect a mixture of products comprising various

deacetylated sugar derivatives. This precursor mixture was dissolved in 0.05 M sodium methoxide methanol solution (3 mL) and the solution was stirred for 12 h at room temperature. After the solution was neutralized using Dowex 50Wx4 (H^+), MPLC purification with a reversed-phase column (water/CH_3OH containing 0.1% TFA) was performed to give the Lewis X-carrying ligand **1a** (40 mg, 58% in 3 steps), which was characterized by NMR spectroscopy (DQF-COSY, HSQC, HMBC, HSQC-TOCSY) and HRMS analyses. HRMS of **1a**: calcd. for $C_{51}H_{71}N_4O_{25}$; 1139.44129, found; m/z 1139.44089 $[M-H]^-$.

Lewis X-containing pentasaccharide **3** was also prepared by deprotection reaction of **4** using sodium methoxide in a quantitative manner.

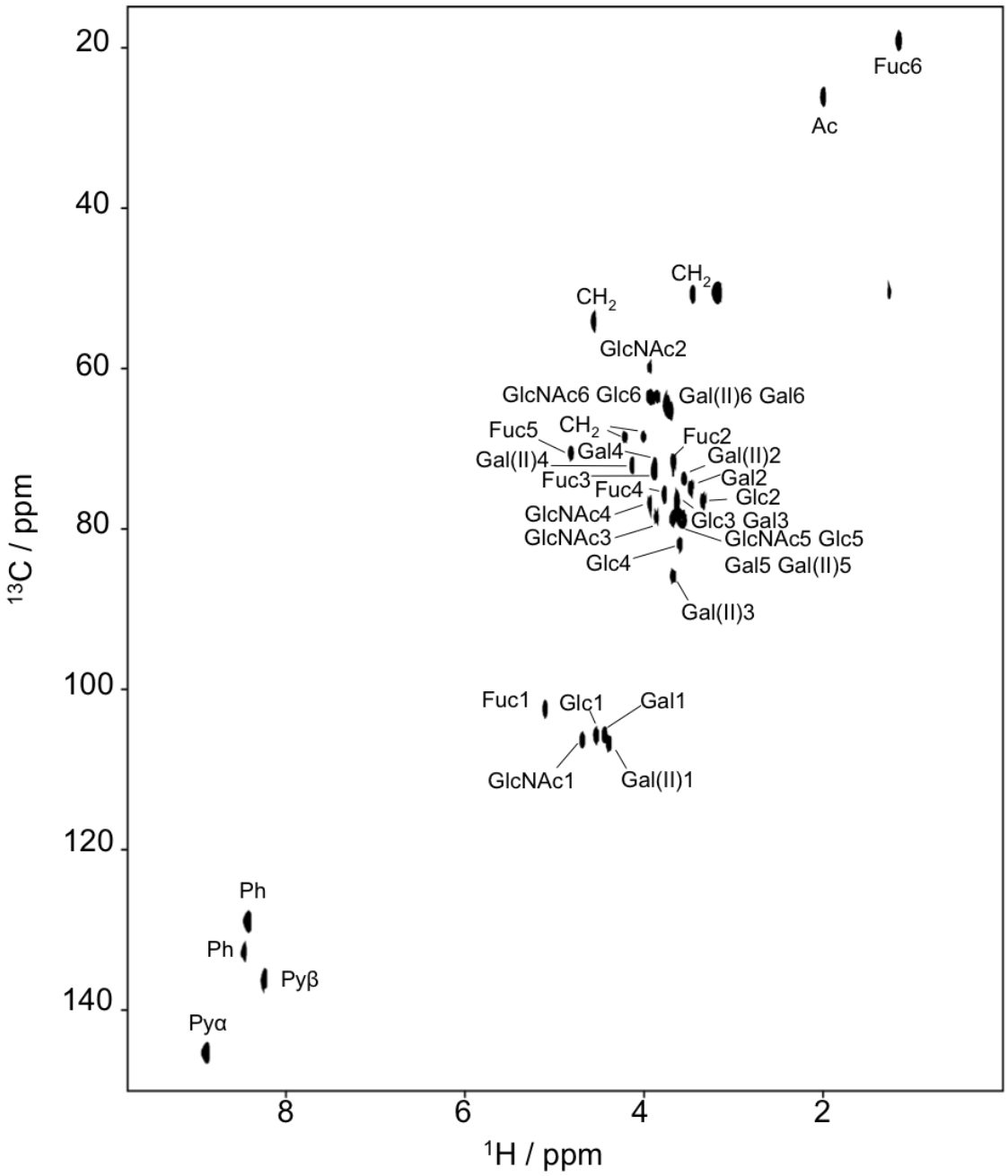

Figure 10. ^{1}H-^{13}C HSQC spectrum of ligand **1a** in D_2O.

Scheme 2. Synthesis of ligand **1b**.

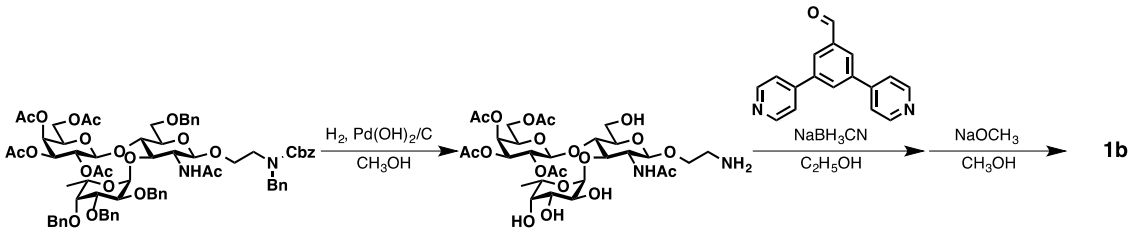

Scheme 3 Synthesis of ligand **1c**.

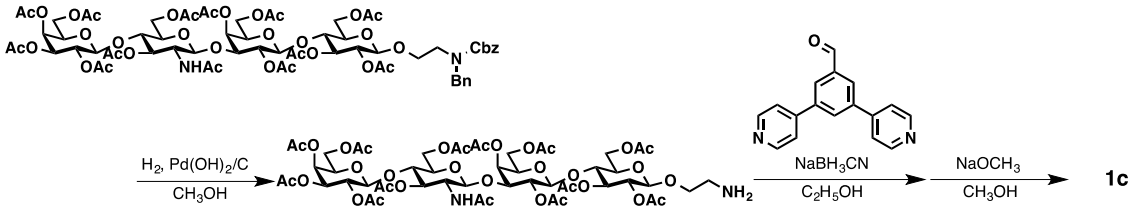

Ligand **1b** and **1c** were prepared following similar protocols as shown in Schemes 2 and 3, respectively. HRMS of **1b**: calcd. for $C_{39}H_{51}N_4O_{15}$; 815.33532, found; m/z 815.33564 $[M\text{-}H]^-$. HRMS of **1c**: calcd. for $C_{45}H_{61}N_4O_{21}$; 993.38338, found; m/z 993.38305 $[M\text{-}H]^-$.

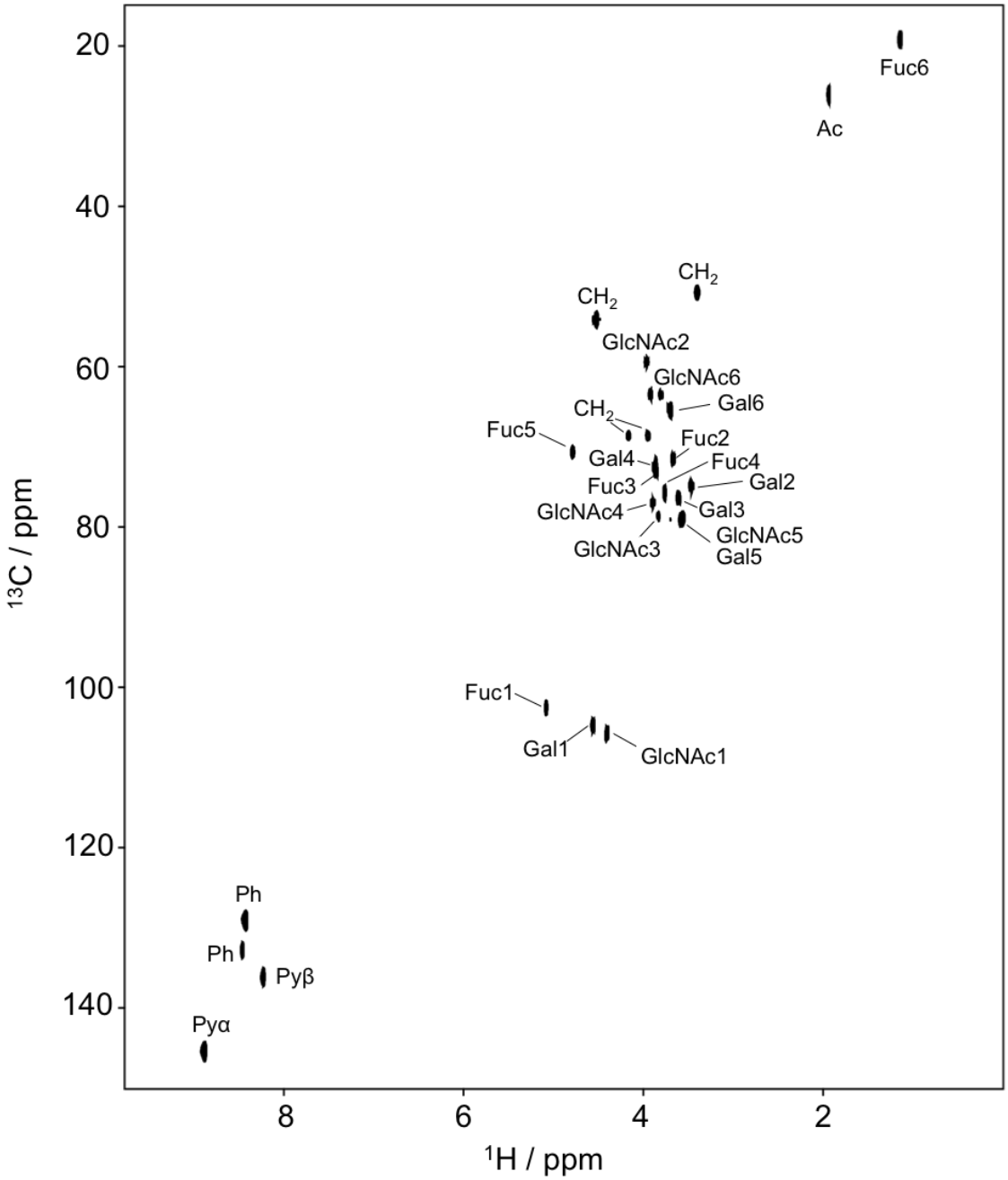

Figure 11. ^{1}H-^{13}C HSQC spectrum of ligand **1b** in D_2O.

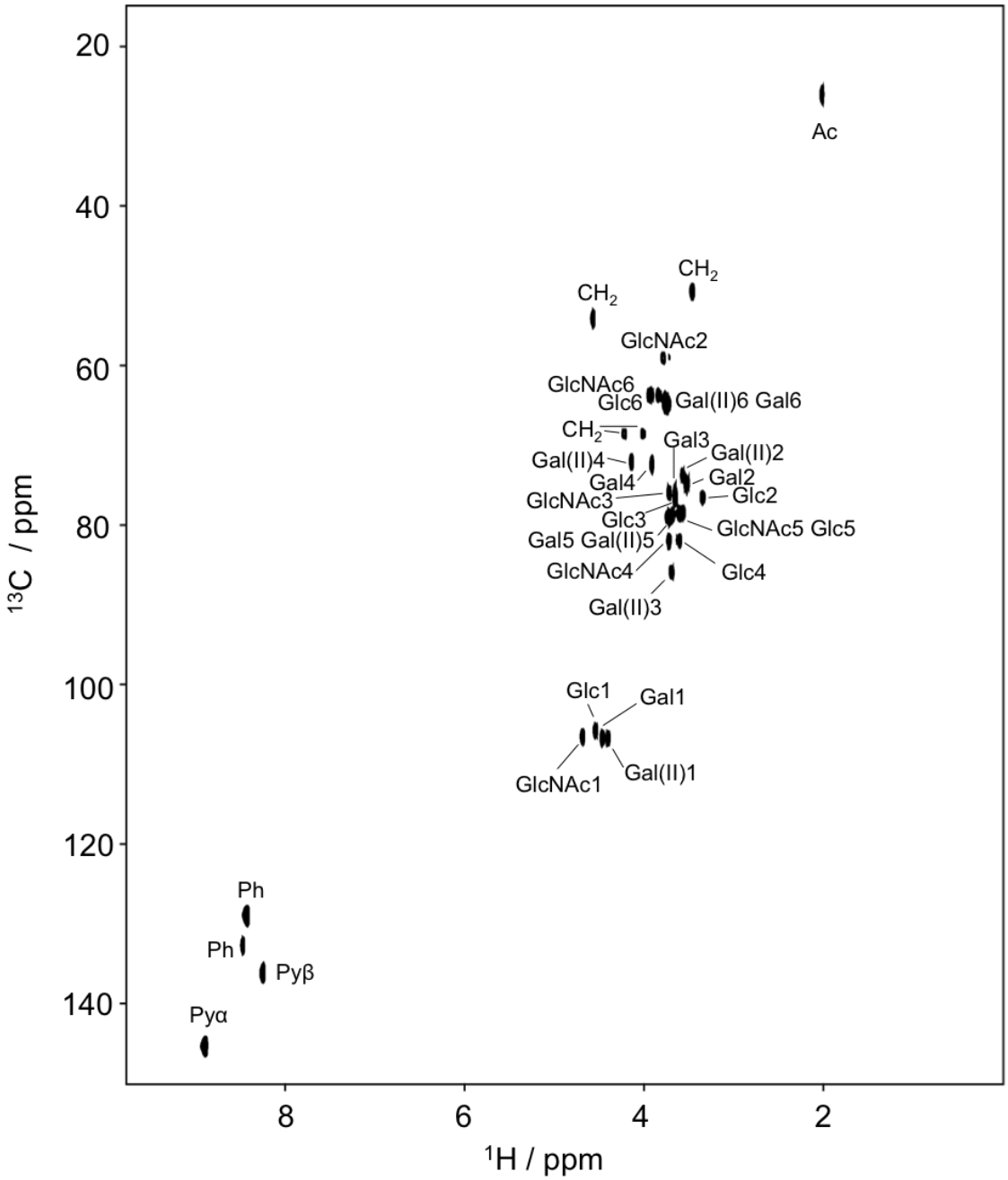

Figure 12. ^{1}H-^{13}C HSQC spectrum of ligand **1c** in D_2O.

References:

1. H. J. Gabius, Eur. J. Biochem. 1997, 243, 543–576.

2. I. Bucior and M. M. Burger, Glycoconj. J. 2004, 21, 111–123.

3. K. Handa and S. Hakomori, Glycoconj. J. 2012, 29, 627–637.

4.C. F. Brewera, M. C. Micelib and L. G Baum, Curr. Opin. Struct. Biol., 2002, 12, 616–623.

5. M. Monsigny, R. Mayer and A. C. Roche, Carbohydr. Lett. 2000, 4, 35–52.

6. R. T. Lee and Y. C. Lee, Glycoconj. J. 2000, 17, 543-551.

7. S. Hakomori, Glycoconj. J. 2004, 21, 125–137.

8. I. Bucior and M. M. Burger, Curr. Opin. Struct. Biol. 2004, 14, 631–637.

9. M. Delbianco, P. Bharate, S. Varela-Aramburu, and P. H. Seeberger, Chem. Rev. 2016, 116, 1693–1752.

10. T. Yamaguchi, T. Uno, Y. Uesaka, M. Yagi-Utsumi and K. Kato, Chem. Commun. 2013, 49, 1235–1237.

11. A. Bernardi, J. Jiménez-Barbero, A. Casnati, C. De Castr, T. Darbre, F. Fieschi, J. Finne, H. Funken, K.-E. Jaeger, M. Lahmann, T. K. Lindhorst, M. Marradi, P. Messner, A. Molinaro, P.l V. Murphy, C. Nativi, S. Oscarson, S. Penadés, F. Peri, R. J. Pieters, O. Renaudet, J.-L. Reymond, B. Richichi, J. Rojo, F. Sansone, C. Schäffer, W. B. Turnbull, T. Velasco-Torrijos, S. Vidal, S. Vincent, T. Wennekes, H. Zuilhof and A. Imberty, Chem. Soc. Rev. 2013, 42, 4709-4727.

12. M. Marradi, F. Chiodo, I. García and S. Penadés, Chem. Soc. Rev. 2013, 42, 4728-4745.

13. K. Matsuura and K. Kobayashi, Glycoconj. J. 2004, 21, 139–148.

14. N. Seah, P. V. Santacroce and A. Basu, Org. Lett. 2009, 11, 559–562.

15. J. M. de la Fuente and S. Penadés, Glycoconj. J. 2004, 21, 149–163.

16. A. C. de Souza, K. M. Halkes, J. D. Meeldijk, A. J. Verkleij, J. F. G. Vliegenthart and J. P. Kamerling, ChemBioChem 2005, 6, 828 –831.

17. N. Jayaraman, K. Maiti and K. Naresh, Chem. Soc. Rev. 2013, 42, 4640–4656.

18. C. Gourier, F. Pincet, E. Perez, Y. Zhang, Z. Zhu, J.-M. Mallet and P. Sinaÿ, Angew. Chem. Int. Ed. 2005, 44, 1683–1687.

19. B. Lorenz, L. Álvarez de Cienfuegos, M. Oelkers, E. Kriemen, C. Brand, M. Stephan, E. Sunnick, D. Yüksel, V. Kalsani, K. Kumar, D. B. Werz and A. Janshoff, J. Am. Chem. Soc. 2012, 134, 3326–3329.

20. A. Kunze, M. Bally, F. Höök and G. Larson, Sci. Rep. 2013, 3, 1452.

21. R. V. Murthy, H. Bavireddi, M. Gade and R. Kikkeri, ChemMedChem, 2015, 10, 792–796.

22. C.-H. Lai, J. Hütter, C.-W. Hsu, H. Tanaka, S. Varela-Aramburu, L. De Cola, B. Lepenies and P. H. Seeberger, Nano Lett. 2016, 16, 807–811.

23. M. Fuss, M. Luna, D. Alcántara, J. M. de la Fuente, P. M. Enríquez-Navas, J. Angulo, S. Penadés, and F. Briones, J. Phys. Chem. B, 2008, 112, 11595-11600.

24. N. Kojima, B. A. Fenderson, M. R. Stroud, R. I. Goldberg, R. Habermann, T. Toyokuni and S. Hakomori, Glycoconj. J. 1994, 11, 238–248.

25. S. Hanashima, K. Kato and Y. Yamaguchi, Chem. Commun. 2011, 47, 10800–10802.

26. A. Geyer, C. Gege and R. R. Schmidt, Angew. Chem. Int. Ed. 2000, 39, 3245–3249.

27. M. J. Hernáiz, J. M. de la Fuente, Á. G. Barrientos, and S. Penadés, Angew. Chem. 2002, 114, 1624–1627.

28. J. M. de la Fuente, P. Eaton, A. G. Barrientos, M. Menéndez, and S. Penadés, J. Am. Chem. Soc. 2005, 127, 6192-6197.

29. K. Harris, D. Fujita and M. Fujita, Chem. Commun. 2013, 49, 6703–6712.

30. D. Fujita, Y. Ueda, S. Sato, N. Mizuno, T. Kumasaka and M. Fujita, Nature 2016, 540, 563–566.

31. K. Suzuki, S. Sato and M. Fujita, Nature Chem. 2010, 2, 25–29.

32. D. Fujita, K. Suzuki, S. Sato, M. Yagi-Utsumi, Y. Yamaguchi, N. Mizuno, T, Kumasaka, M. Takata, M. Noda, S. Uchiyama, K. Kato and M. Fujita, Nature Commun. 2012, 3, 1093.

33. N. Kamiya, M. Tominaga, S. Sato and M. Fujita, J. Am. Chem. Soc. 2007, 129, 3816–3817.

34. S. Sato, Y. Yoshimasa, D. Fujita, M. Yagi-Utsumi, T. Yamaguchi, K. Kato and M. Fujita, Angew. Chem. Int. Ed. 2015, 54, 8435–8439.

35. M. Utsumi, Y. Yamaguchi, H. Sasakawa, N. Yamamoto, K. Yanagisawa and K. Kato, Glycoconj. J. 2009, 26, 999–1006.

36. R. Sharp, L. Lohr and J. Miller, Progr. Nucl. Magn. Reson. Spectrosc. 2001, 38, 115–158.

37. B. Henry, H. Desvaux, M. Pristchepa, P. Berthault, Y.-M. Zhang, J.-M. Mallet, J. Esnault and P. Sinaÿ, Carbohydr. Res. 1999, 315, 48-62.

Chapter 4: Creation of Lewis X-carrying neoglycolipids for controlling cellular functions

This chapter is adapted and modified from Hirokazu Yagi, Gengwei Yan, Tatsuya Suzuki, Shingo Tsuge, Takumi Yamaguchi, and Koichi Kato, "Lewis X-Carrying Neoglycolipids Evoke Selective Apoptosis in Neural Stem Cells," Neurochem. Res. 2017, DOI: 10.1007/s11064-017-2415-5.

4.1 Introduction

Accumulating evidence has highlighted the importance of carbohydrate–protein and carbohydrate–carbohydrate interactions in cellular communication, as demonstrated by carbohydrate-mediated cell recognition in embryonic and tumor cells [1]. The functional significance of glycan-mediated molecular events on cell surfaces has been reported in adhesion and migration of neuronal cells, including neural stem cells (NSCs) [2]. Comprehensive glycosylation profiling of NSCs has revealed that glycosylation patterns in NSCs are significantly altered during differentiation [3]. For example, Lewis X-carrying oligosaccharides are exclusively expressed in the predifferentiated state. In particular, the Lewis X glycotope has long been recognized as an undifferentiation marker and has been identified in several glycoproteins in NSCs [4-6]. Moreover, Lewis X-carrying oligosaccharides have been shown to be positively involved in the activation of the Notch signaling pathway and thereby actively contribute to the maintenance of stemness in NSCs [6]. This functional pathway is supposed to be activated by oligosaccharide recognition on the NSC surface.

However, it is still remaining as tasks with more challenge to modify the carbohydrate functions of the cell membranes and thereby control cellular functions. In the present study, I sought to address the functional roles of Lewis X-mediated molecular interactions on NSCs using an artificial glycocluster displaying Lewis X glycotopes. Therefore, I created neoglycolipids in which the Lewis X group was combined with acyl chain derivatives to mimic the glycolipid clusters displayed on

the NSC surface for exploring possible bioactivity of synthetic glycoclusters.

4.2 Results and Discussion

To create a functional cluster of Lewis X, I conjugated the trisaccharide with an acyl chain using lactose as a spacer, giving rise to a pentasaccharide-displaying neoglycolipid (neoglycolipid **1** in Figure 1). The synthesis of neoglycolipid **1** was shown in Figure 1. As a reference, neoglycolipid **2** devoid of the fucose residue and the pentasaccharide with an acetyl moiety (neoglycolipid **3**) was also prepared.

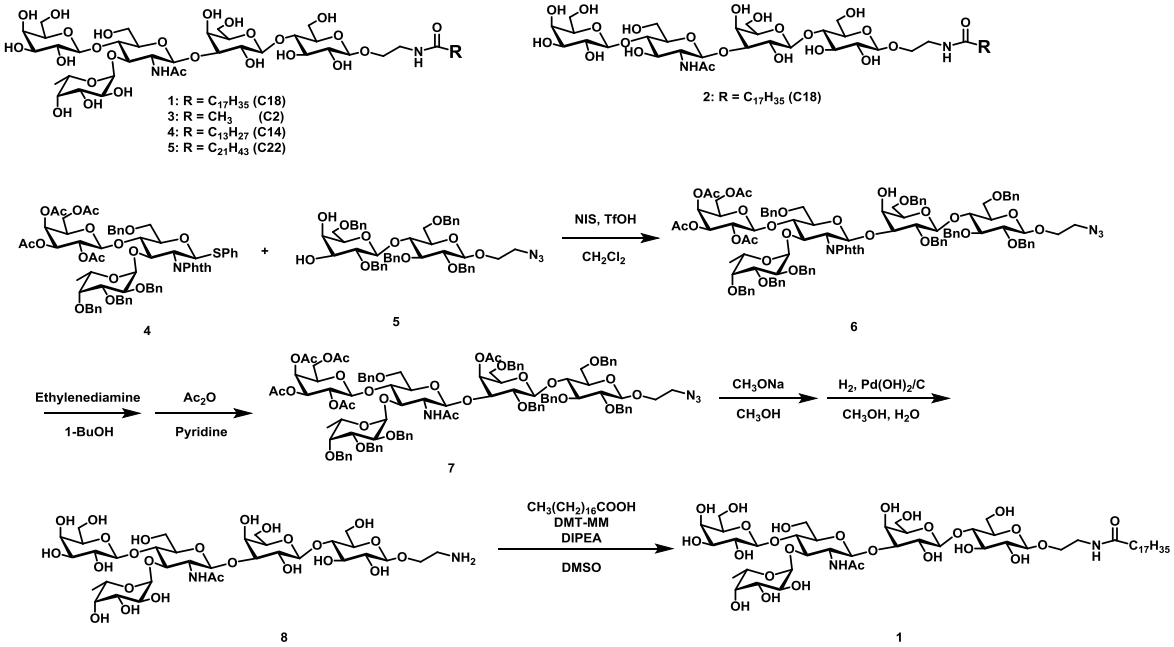

Figure 1. The structures of neoglycolipids prepared in this study and the synthesis of neoglycolipid **1**.

DLS measurements showed that neoglycolipids **1** and **2** assembled into micellar forms in aqueous conditions (Figure 2), whereas the pentasaccharide with the acetyl group did not. The neoglycolipid underwent hyper-assembly on addition of Ca^{2+} ions, depending on the presence of the fucose residue, consistent with the observation for the glycoclusters formed with a metal-organic complex and penta- or tetra-oligosaccharides [7]. These results confirmed that the designed neoglycolipid clusters displayed the functional Lewis X glycotope on their surfaces.

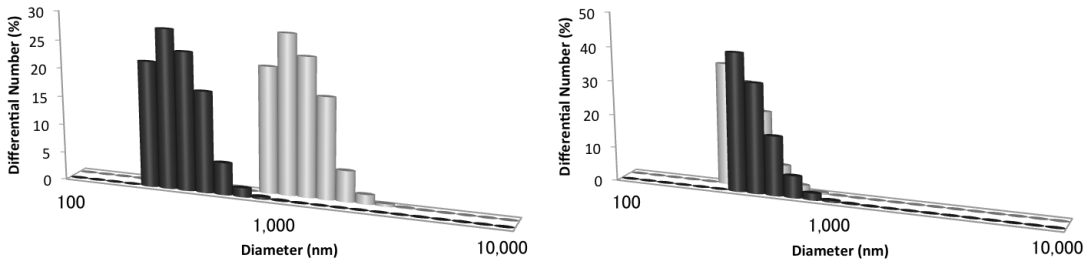

Figure 2. Size distributions observed in DLS measurements of 1 mM aqueous solution of (a) neoglycolipid **1** and (b) negoglycolipid **2** in the absence (black) and presence (gray) of Ca^{2+} ions (100 mM).

The effects of the neoglycolipids on cell proliferation were estimated by applying them to NCSs before and after differentiation. Surprisingly, the Lewis X-carrying neoglycolipid evoked selective apoptosis in undifferentiated NSCs, whereas differentiated neuronal cells remained unaffected (Figure 3). Apoptosis in undifferentiated NSCs was suppressed by the removal of the acyl moiety or

the fucose residue from the Lewis X-carrying neoglycolipid, indicating that the functional Lewis X group in a clustered form was a prerequisite for apoptosis (Figure 3a).

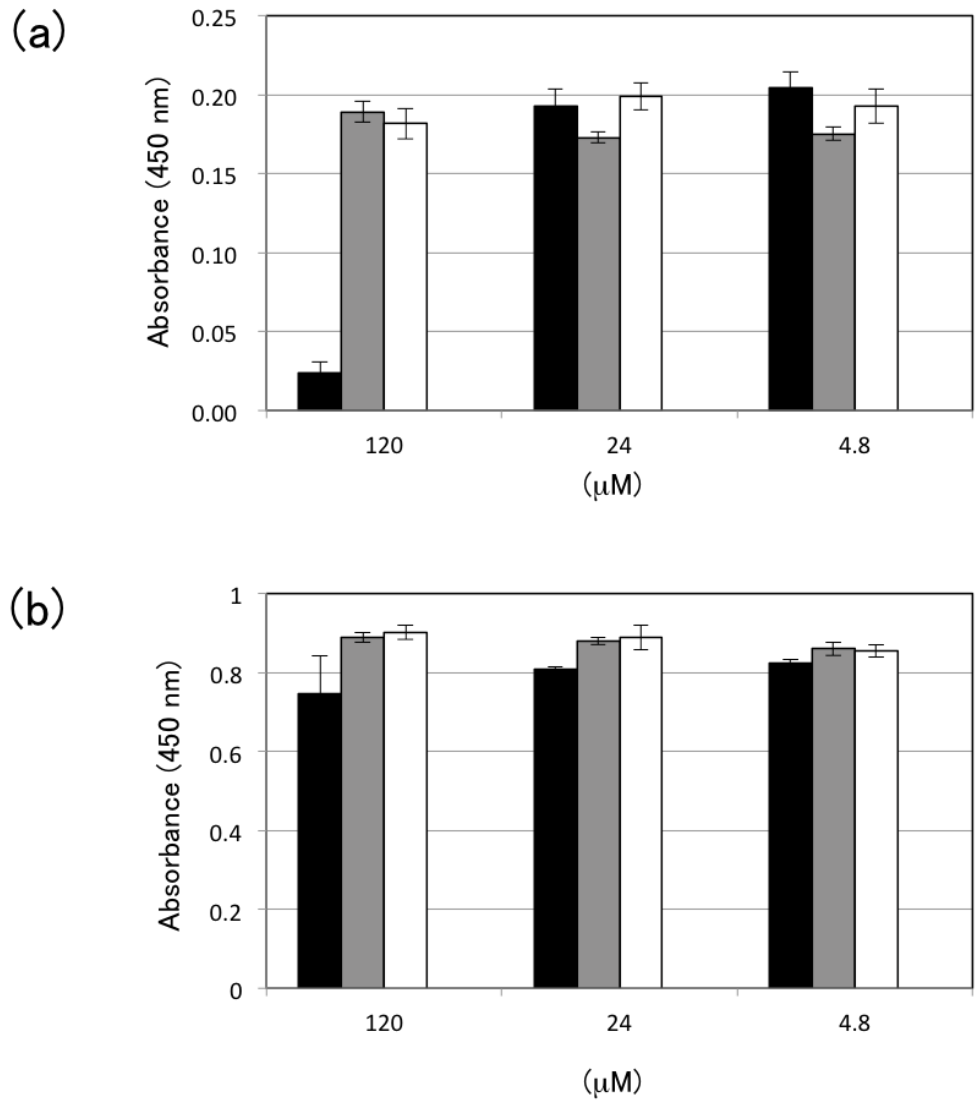

Figure 3. Cell viability assay performed using neoglycolipids **1** (black), **2** (gray) and **3** (white). The synthetic compounds were applied to NSCs (a) before and (b) after differentiation.

The dependence of this activity on the acyl chain length of neoglycolipid was also examined. The Lewis X-carrying pentasaccharide was conjugated with

C14 or C22 acyl chains (Figure 1). The apoptotic activities of these neoglycolipids were compared with that of the C18 analog. Interestingly, the apoptotic activity of the Lewis X-carrying neoglycolipid depended on the length of the acyl chain, with the optimum length being C18 (Figure 4).

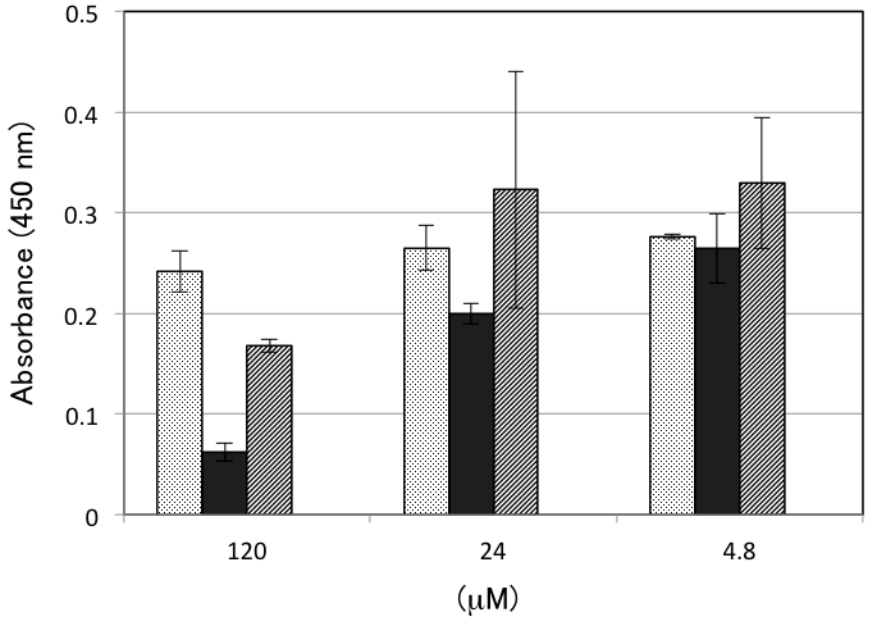

Figure 4. Apoptosis induced assay performed using pentasaccharide neoglycolipid with C14 (**4**) (dotted), C18 (**1**) (black) and C22 (**5**) (striped) acryl moieties. The synthetic neoglycolipids were applied to NSCs.

A possible mechanism for this apoptotic activity of the neoglycolipid clusters is suggested. Dendritic cell-specific ICAM-3 grabbing non-integrin (DC-SIGN) is a scavenger receptor lectin and functions in endocytosis through interaction with Lewis X-expressing glycoproteins [8]. Although DC-SIGN is not predominantly expressed in NSCs, a specific lectin C1qR1 is expressed,

which is an undifferentiation marker [9]. Furthermore, several endocytosis-related cell surface molecules specifically expressed on NSCs, such as perlcan [10,11], which have the potential to recognize carbohydrate moieties [2]. Based on those reports, it is plausible that these proteins are expressed exclusively on predifferentiated NSC surfaces and specifically bind the Lewis X-carrying neoglycolipid clusters, thereby mediating endocytotic uptake. The neoglycolipid contains an amide bond, which can be cleaved once it is taken up by the cells, releasing free fatty acids. Intracellular accumulation of long-chain saturated free fatty acids (i.e., C16:0 and C18:0) has been shown to induce apoptosis in several cell types [12,13]. The acyl chain length dependence of apoptotic activity observed for the neoglycolipid that I prepared is consistent with a report on fatty acid-induced cell death effects in microvascular mesangial cells [12].

4.3 Conclusions

For designing and creating glycoclusters having new functionality, Lewis X-carrying neoglycolipids were synthesized as tools for controlling cellular functions. A property of a neoglycolipid that I prepared, which is composed of a Lewis X-containing pentasaccharide and a C18 acyl chain, was discovered. A hypothetical functional mechanism of the neoglycolipid involving selective NSC targeting with the Lewis X oligosaccharide and apoptotic signaling, due to the intracellularly released fatty acids. These finding may offer a new strategy for controlling neural cell fates

using artificial glycoclusters.

4.4 Materials and Experiments

4.4.1 General

The Lewis X-carrying neoglycolipids were chemically synthesized from glucosamine, fucose, galactose, and lactose building blocks, obtained from TCI Co. All other reagents and solvents were purchased from TCI Co., WAKO Pure Chemical Industries, KANTO Chemical Co., and Sigma-Aldrich Co.

High resolution mass spectrometry (HRMS) analyses were performed at the Instrumental Center in Institute for Molecular Science. DLS measurements were performed using an Otsuka Electronics ELSZ-1000 particle analyzer at room temperature.

4.4.2 Synthesis of neoglycolipids

To a suspended solution of compound **4** (120 mg, 97 μmol), compound **5** (70 mg, 81μmol), NIS (22 mg, 97 μmol), and 3 Å molecular sieves (500 mg) in CH_2Cl_2 (5 mL), TfOH (1 μL, 10 μmol) were added drop-wise and the mixture was stirred for 6 h at -35°C. The reaction mixture was filtered through celite. The filtrate was diluted with $CHCl_3$, and the organic phase was washed with aqueous $Na_2S_2O_3$, saturated aqueous $NaHCO_3$, dried over Na_2SO_4, and concentrated. The residue was purified with a SNAP Ultra column using a Biotage Isolera medium-pressure liquid chromatography (MPLC) system to yield the pentasaccharide derivative **6** (90 mg,

56%).

Compound **6** (90 mg, 45 μmol) was suspended in 1-butanol (5 mL) with ethylenediamine (1 mL, 15 mmol), and the mixture was stirred for 18 h at 85°C. The crude product was dissolved in pyridine (6 mL), and acetic anhydride (5 mL, 53 mmol) was added drop-wise to the solution, placed in an ice-water bath. After stirring for 15 h at 50°C, the reaction mixture was cooled to room temperature and concentrated. The residue was diluted using ethyl acetate, and the organic phase was washed with 1_N aqueous HCl, H_2O, saturated aqueous $NaHCO_3$, dried over Na_2SO_4, and concentrated. The residue was purified using the MPLC system with a SNAP Ultra column to yield compound **7** (50 mg, 58%).

Compound **7** (25 mg, 13 μmol) was mixed with sodium methoxide (3 mg, 60 μmol) in methanol (5 mL). After stirring for 12 h at room temperature, the solution was neutralized with Dowex 50WX4 cation exchange resin. The crude product was dissolved in methanol with water, and $Pd(OH)_2/C$ (100 mg) was added to the solution. The reaction mixture was stirred for 24 h at room temperature in an atmosphere of H_2. The mixture was filtered through celite and concentrated. Subsequently, the solution was applied to a GE PD minitrap G-10 column to remove the salt and then concentrated to yield compound **8** (10 mg, 85%).

The mixture of stearic acid (3 mg, 11 μmol), DMT-MM (3 mg, 11 μmol), and DIPEA (50 μL, 287 μmol) in DMSO (2 mL) was stirred for 10 min at room temperature and transferred to a solution of compound **8** (10 mg, 11 μmol) in DMSO (1 mL). After stirring for 12 h at room temperature, the reaction mixture was purified

using a Waters Sep-Pak C18 column and then a GE PD minitrap G-10 column to yield neoglycolipid **1** (4 mg, 30%), which was characterized by NMR and HRMS analyses. HRMS (FAB); Calcd for $C_{52}H_{95}N_2O_{26}$ $[M+H]^+$: 1163.6168; Found: 1163.6193.

Neoglycolipid **2** was synthesized in a similar manner, as summarized in scheme 2. HRMS (FAB) of **2**; Calcd for $C_{46}H_{85}N_2O_{22}$ $[M+H]^+$: 1017.5588; Found: 1017.5610.

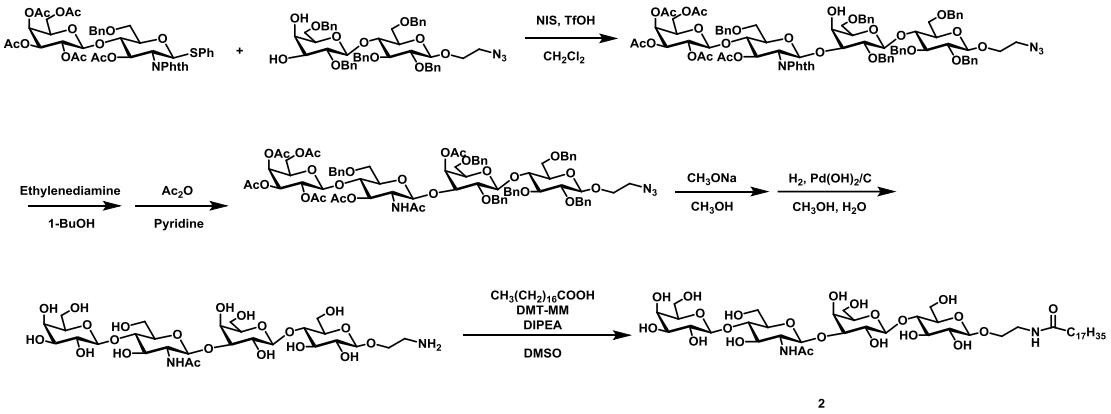

Scheme 2. Synthesis of neglycolipid **2**.

4.4.3 Cell viability assay

Cell viability after addition of the neoglycolipids was analyzed using the WST-8 reagent [2-(2-methoxy-4-nitrophenyl)-3-(4-nitrophenyl)-5-(2,4-disulfophenyl)-2H-tetrazolium, monosodium salt] (Dojindo Molecular technologies Inc.). The assay is based on the cleavage of the tetrazolium salt WST-8 by cellular dehydrogenases in viable cells. The spectrophotometric absorbance of the WST-8-formazan produced by dehydrogenase activity in the living cells was measured at 450 nm (reference,

650 nm), using a microplate spectrophotometer.

References:

1. N. Kojima, B. A. Fenderson, M. R. Stroud, R. I. Goldberg, R. Habermann, T. Toyokuni, S. Hakomori, Glycoconj J, 1994, 11, 238-248.

2. R. Kleene and M. Schachner, Nat Rev Neurosci, 2004, 5, 195-208.

3. H. Yagi and K. Kato, Glycoconj J, 2016, DOI: 10.1007/s10719-016-9707-x

4. E. Hennen, D. Safina, U. Haussmann, P. Worsdorfer, F. Edenhofer, A. Poetsch, A. Faissner, J Biol Chem, 2013, 288, 16538-16545.

5. H. Yagi, T. Saito, M. Yanagisawa, R. K. Yu, K. Kato, J Biol Chem, 2012, 287, 24356-24364.

6. H. Yagi, M. Yanagisawa, K. Kato, R. K. Yu, Glycobiology 2010, 20, 976-981.

7. G. Yan, T. Yamaguchi, T. Suzuki, S. Yanaka, S. Sato, M. Fujita, K. Kato, Chem Asian J 2017, 12, 968-972.

8. P. J. Coombs, S. A. Graham, K. Drickamer, M. E. Taylor, J Biol Chem 2005, 280, 22993-22999.

9. Y. H. Yu, G. Narayanan, S. Sankaran, S. Ramasamy, S. Y. Chan, S. Lin, J. Chen, H. Yang, H. Srivats, S. Ahmed, Stem Cells Dev 2016, 25, 189-201.

10. I. V. Fuki, R. V. Iozzo, K. J. Williams, J Biol Chem 2000, 275, 25742-25750.

11. A. Kerever, F. Mercier, R. Nonaka, S. de Vega, Y. Oda, B. Zalc, Y. Okada, N. Hattori, Y. Yamada, E. Arikawa-Hirasawa, Stem Cell Res 2014, 12, 492-505.

12. R. Mishra, M. S. Simonson, Cardiovasc Diabetol 2005, 4, 2

13. L. L. Listenberger, D. S. Ory, J. E. Schaffer, J Biol Chem 2001, 276, 14890-14895.

Chapter 5. Conclusion and perspective

In this thesis, I characterized the dynamic interactions involving the Lewis X-derived oligosaccharides, including their conformational adaptation to the binding proteins as well as the multivalent recognition, by hybridizing biophysical, synthetic, and biochemical approaches.

In chapter 2, I characterized the conformational dynamics of the Lewis X oligosaccharide by employing the lanthanide-assisted NMR technique combined with molecular simulation. The results in conjunction with the previously reported crystallographic data revealed the lectins selected rare conformers of Lewis X during binding processes. This finding motivated me to re-design its conformational space for controlling its protein-binding properties. Indeed, chemical modification of the Lewis X trisaccharide to populate the bound conformations successfully improved its protein-binding affinity. Thus, remodeling of the conformational spaces of oligosaccharides is an effective methodology for designing artificial oligosaccharides with improved efficacy through better understanding of their conformational dynamics.

In chapter 3, I hybridized the Lewis X oligosaccharide with the self-assembled metal-organic complex for creating neoglycoclusters, which possess structural homogeneity suitable for structural analyses and also potential functional ability through multivalent interaction. The well-defined Lewis X clusters enabled detailed NMR characterization of their interactions mediated by the oligosaccharides moieties. My NMR data revealed that the specific carbohydrate structure as well as their clustering form are prerequisite for the Ca^{2+}-mediated

carbohydrate-carbohydrate interaction.

Moreover, in chapter 4, I created the novel glycoclusters composed of Lewis X-carrying neoglycolipids as tools for controlling cellular functions. In this approach, it was demonstrated that the Lewis X-carrying neoglycolipid evoked selective apoptosis in undifferentiated neural stem cells, whereas differentiated neuronal cells remained unaffected.

Thus, I employed synthetic approach integrated with biopysical techniques including NMR spectroscopy. Consequently, I could successfully design and create the neo-glycomolecules by hybridizing biomolecules and artificial molecules. The dynamical structures and assembly states of these neo-glycomolecules are artificially controlled in attempt to endow them with the higher affinity for target proteins, the Ca^{2+}-mediated hyper-assembling property, and the selective apoptotic activity. It is expected that these neo-glycomolecules can be useful tools for probing protein-carbohydrate interactions, carbohydrate-carbohydrate interactions, and cellular functional processes. It is also expected that the strategy I developed for creation and characterization of the neo-glycomolecules can be applicable for other biomolecules with structural flexibility and assembling properties.

Acknowledgments

I feel much indebted to many people who have instructed and favored me in the course of writing this. First of all, I would like to express my sincere heartfelt thanks to my supervisor Prof. Koichi Kato for giving me the opportunity to join the wonderful group and for his professional guidance, constant support and patience in supervisions. I admire his profound knowledge and brilliant view on science, I benefited greatly from his lecture and the discussion with him, from these I realized how to be a scientist and professor. Then I would like to express my thanks to Dr. Takumi Yamaguchi for his immense help for teaching me the experimental skills and discussing for solving the problems. His insightful view and warm-heart encouragement guided me in the whole process of my research career.

The members of Prof. Kato's group all helped me a lot during my research. I would like to thank Dr. Hirokazu Yagi for teaching me the cell viability test and the insightful knowledge about the Lewis X saccharide. I also want to thank Dr. Tatsuya Suzuki for teaching me the experimental skills and sharing the experiences in oligosaccharide synthesis research. I am grateful for Dr. Saeko Yanaka for teaching me analyzing the NMR results. Thanks to Dr. Tadashi Satoh for teaching me the knowledge about the functioning mechanisms of proteins and glycoconjugates. I would like to thank Dr. Maho Yagi-Utsumi for her brilliant opinion on discussion about my research work and presentations. Thanks to Dr. Kensuke Kurihara for teaching me performing the DLS measurements. Thanks to Dr. Kentaro Ishii for

teaching me performing the mass experiments. Thanks to Dr. Ying Zhang and Mr. Jinzheng Wang for teaching the experimental skills when I just joined the lab. I would like to thank all the previous and present lab members in IMS and NCU, all of them are friendly and cooperative. They helped me not only in my research but also in my daily life. They are Dr. Tong Zhu, Dr. Satoshi Ninagawa, Mr. Takahiro Anzai, Dr. Yinghui Wang, Dr. Arunima Sikdar, Mr. Koya Inagaki, Mr. Yasuhiro Yunoki, Ms. Rina Yogo, Ms. Methanee Hiranyakorn, Dr. Ratsupa Thammaporn, Dr. Supaporn Seetaha. Technicians and secretaries; Ms. Yukiko Isono, Ms. Hiroe Naito, Ms. Tomo Okada, Ms. Kei Tanaka.

Also I want to thank the members of Yamaguchi lab in JAIST, thanks to Mr. Yoshiki Hori, Mr. Shingo Murakami and Mr. Qiang Xu for sharing the experiment room and have the great time together.

Furthermore, I would like to thank Dr. Sota Sato (The University of Tokyo), Prof. Makoto Fujita (The University of Tokyo) and his group members Dr. Tomohisa Sawada and Dr. Daishi Fujita for useful discussion and cooperation in preparing metal-organic complex. I would like to thank Dr. Hiroaki Tateno (AIST) for conducting FAC measurements.

I sincerely appreciate the examiners of this thesis; Prof. Shigetoshi Aono, Prof. Shigeyuki Masaoka, Prof. Katsuyuki Nishimura (IMS), and Prof. Yoshiki Yamaguchi (RIKEN).

Lastly, I especially thank my mom and my dad, my gratitude also extends to my family who have been assisting, supporting and caring for me all of my life.